

A generalized statistical model for fits to parton distributions

Mengshi Yan,¹ Tie-Jiun Hou,² Zhao Li,^{3,4} Kirtimaan Mohan,^{5,*} and C.-P. Yuan⁵

¹*Department of Physics and State Key Laboratory of Nuclear Physics and Technology,*

Peking University, Beijing 100871, China.[†]

²*School of Nuclear Science and Technology,*

University of South China, Hengyang 421001, China.[‡]

³*Institute of High Energy Physics, Chinese Academy of Sciences, Beijing 100049, China;*

School of Physics Sciences, University of Chinese Academy of Sciences, Beijing 100039, China

⁴*Center for High Energy Physics, Peking University, Beijing 100871, China.*[§]

⁵*Department of Physics and Astronomy, Michigan State University, East Lansing, MI 48824, U.S.A.*[¶]

(Dated: June 5, 2024)

Parton distribution functions (PDFs) form an essential part of particle physics calculations. Currently, the most precise predictions for these non-perturbative functions are generated through fits to global data. A problem that several PDF fitting groups encounter is the presence of tension in data sets that appear to pull the fits in different directions. In other words, the best fit depends on the choice of data set. Several methods to capture the uncertainty in PDFs in presence of seemingly inconsistent fits have been proposed and are currently in use. These methods are important to ensure that uncertainty in PDFs are not underestimated. Here we propose a novel method for estimating the uncertainty by introducing a generalized statistical model inspired by unsupervised machine learning techniques, namely the Gaussian Mixture Model (GMM). Using a toy model of PDFs, we demonstrate how the GMM can be used to faithfully reconstruct the likelihood associated with PDF fits, which can in turn be used to accurately determine the uncertainty on PDFs, especially in presence of tension in the fitted data sets. We further show how this statistical model reduces to the usual chi-squared likelihood function for a consistent data set and provide measures to optimize the number of Gaussians in the GMM.

* kamohan@msu.edu

† msyan@pku.edu.cn

‡ tjhou@msu.edu

§ zhaoli@ihep.ac.cn

¶ yuanch@msu.edu

CONTENTS

I. Introduction	3
II. Tension in a toy model	6
II.1. Two pseudo-data sets with tension	6
II.2. Least Squares Fits and Tension	7
III. Gaussian mixture model in PDF fit	11
III.1. Performing parameter fits with the GMM	13
III.2. Mean and Uncertainty in the GMM	15
IV. Application of the GMM in a toy model of PDFs	17
IV.1. Applying GMM to different scenarios	18
IV.2. The GMM method compared to different tolerance criteria	22
V. Consistency checks for the GMM	26
V.1. Consistent results from consistent data	27
V.2. Information Criteria for an Optimal number of base Gaussians	29
VI. Conclusion	32
Acknowledgment	34
References	34

I. INTRODUCTION

Parton distribution functions (PDFs) are non-perturbative functions quantifying the probability of finding a quark or gluon with certain momentum fraction x from a nucleon. Taking advantage of a wide variety of experimental data and advanced computing packages for perturbative QCD (and electroweak) calculations, various groups [1–5] provide a sophisticated determination of PDFs. The recently released NNPDF [6] and `xFitter` [7] fitting codes open opportunities for general users to also conduct global QCD analyses.

These PDFs form a critical component of the theory community’s infrastructure [8] and developing the next generation of PDFs are crucial for achieving the physics goals of the Large Hadron Collider (LHC) and the Electron-Ion Collider (EIC). An unbiased determination of PDFs are essential for precision phenomenology and the search for new physics, such as the recent measurement of W boson mass by the CDF collaboration [9]. A robust understanding of the the uncertainties arising from PDFs is necessary to provide precise predictions. PDF uncertainties constitute one of the dominant systematic errors both for direct searches of new physics [10] and for precision tests of the Standard Model (SM), such as determining the properties of the Higgs boson [11]. A faithful determination of PDFs and its uncertainties are thus necessary in order to make precise theory predictions at hadron-hadron and lepton-hadron colliders. Improving PDFs will require new experimental data, new theoretical (higher-order) calculations and a determination of fits to global data in a statistically robust way [8].

Many issues could be encountered when trying to perform global fits to data sets from a variety of experiments. One of these issues, which is the primary focus of this paper, is in dealing with data that appear to be in tension with each other, leading to inconsistencies within the global fit. For example, suppose we have two data sets that pull the fit parameters to different values. In this scenario, the data are in tension with each other. The source of such tension could arise due to deficiencies in theoretical models and calculations or even from underestimation of experimental uncertainties. To keep the discussion simple, we work with an example of the latter, although, the method presented here is agnostic to the source of tension.

An example of tension between data sets would be the measurement of the ATLAS 8 TeV W and Z rapidity distribution [12], which was found to be inconsistent with other data included in the PDF global analysis and favored an enhanced strange quark distribution function [1, 2, 13]. Although a non-vanishing strangeness asymmetry $(s - \bar{s})(x)$ can partially release this tension [2, 13],

it is still inadequate to accommodate the ATLAS 8 TeV W/Z data [12] consistently in a PDF global analysis.

Another example is the inconsistency between the E866 NuSea and E906 SeaQuest measurements of the cross-section ratio $\sigma(pd)/2\sigma(pp)$, which approximates the ratio of anti-quark PDFs $\sigma(pd)/2\sigma(pp) \approx (1 + \bar{d}_p(x_2)/\bar{u}_p(x_2))/2$. The E866 NuSea and E906 SeaQuest measurements provide valuable information on the PDF ratio $(\bar{d}/\bar{u})(x)$ in the large- x region. However, they are found to be in tension at large- x [13–15]. The effect of tension between certain data sets generally becomes negligible for large data sets, when outliers appear with small probability. However, in this case, E866 NuSea and E906 SeaQuest, the measurements probe a specific kinematic region that is otherwise weakly constrained and hence the tension between them cannot be ignored. It is thus necessary to develop a prescription to accommodate such inconsistencies in a PDF global analysis in order to properly estimate the PDF uncertainty.

Several methods have been proposed and are currently in use to provide an estimate of uncertainties especially in the presence of tension[16]. One naive approach would be to simply omit one of the troublesome data sets or perhaps attach a significantly lower weight to this data set. This approach introduces biases in the fitting procedure that needs to be justified with some prior knowledge. In some cases, such a justification may be possible. For example, if perhaps the methodology of the omitted experiment is analyzed and found to be unsatisfactory. In such a scenario, the prior bias in omitting the data set from this experiment is justified, but this is not always the case, since it is not always straightforward to reanalyze particle physics experiments and their data.

Modern PDFs perform fits to data by defining a likelihood or loss function. For PDFs produced by CTEQ-TEA (CT) [1] and MSHT [2], the likelihood is the $\Delta\chi^2$. Under normal circumstances with a consistent set, the uncertainty can be defined by the 68% confidence level limit of the χ^2 distribution, which amounts to varying the fit and determining boundaries where $\Delta\chi^2 = 1$. The advanced methodology adopted by both CTEQ-TEA and MSHT is to introduce a tolerance T such that the fits should be varied within $\Delta\chi^2 = T^2$. Values of T are chosen either dynamically [2] or set to a fixed value [1]. Typical values of T are much larger than 1, which increases the uncertainties in the PDFs. NNPDF uses the Monte-Carlo method for determining uncertainties, where they produce representative sample of PDFs by sampling their likelihood or loss function with the help of pseudo-data, which might be one of the reasons for the uncertainties from NNPDF’s analysis being notably different [17]. Although, as pointed out in Refs. [18–20], the level of inconsistency with data sets is found to be negligible in the NNPDF3.1 analyses, further study is needed to understand

differences between NNPDF and the other fitting groups. One such task was performed in Ref. [21], which details benchmark comparisons of three global PDF sets - CT18, MSHT20 and NNPDF3.1 - and their similarities and differences that have been observed. The end result of that study was a new PDF4LHC21 ensemble of combined PDFs suitable for a wide range of LHC applications.

In this paper we describe how to apply a more general statistical framework to accommodate potential inconsistencies in PDF data. Specifically, we show how the Gaussian Mixture Model (GMM), which is commonly used as an unsupervised machine learning technique, can be adapted to produce PDF uncertainties that faithfully represent the likelihood of PDF fits. Our major findings are summarized below for the benefit of the reader.

- The Least Squares(LS) method is based on the assumption that the likelihood function looks like a single Gaussian distribution. Thus the likelihood is not faithfully represented when dealing with inconsistent data sets. The resulting uncertainties can be highly overestimated in some regions whereas they can simultaneously be highly underestimated in other regions.
- The GMM provides a way to faithfully represent the likelihood of a combination of data sets with tension, which in turn gives a more accurate estimate of uncertainties. Therefore, the implementation of GMM in the PDF global fitting can be expected to accommodate the data sets with varying degrees of tension.
- It is necessary to assess the level of tension in the data sets and to determine the optimal hyperparameters of the GMM. We use the Akaike Information Criterion (AIC) and Bayesian Information Criterion (BIC) to make such a determination and avoid either over-fitting or under-fitting.

The rest of the paper is organized as follows. In Sec. II, we set up a toy PDF model and describe different pseudo-data sets, some of which have obvious tension between them. Section III introduces the Gaussian Mixture Model as the statistical model to be used in order to deal with inconsistencies in data sets. In Sec. IV, the results of the GMM fit are compared with those of conventional fits using the usual least squares fit. Consistency between the GMM and the commonly-used Least Squares (LS) method is evaluated using a data set with no tension in Sec. V. Finally, we discuss our results and conclude in Sec. VI.

II. TENSION IN A TOY MODEL

In this section we introduce a toy model of PDFs and perform LS fits in order to illustrate issues that arise when there is tension between data sets.

II.1. Two pseudo-data sets with tension

We begin by utilizing the toy model of pseudo-PDF suggested in Ref. [22] and choose the functional form of the underlying truth to be,

$$g(x) = a_0 x^{a_1} (1-x)^{a_2} e^{xa_3} (1+xe^{a_4})^{a_5}. \quad (2.1)$$

Here $\{a_0, a_1, a_2, a_3, a_4, a_5\}$ are parameters of the function. To keep the discussion clear we will only perform fits to subsets of these parameters, while keeping others fixed. We would like to emphasize that although we choose an explicit functional form, the starting point could have also been a deep neural network or a polynomial parametrization.¹ Here, we restrict ourselves to use only the functional form in Eq. (2.1) for clarity of presentation.

We generate pseudo-data sets by setting values of the parameters a_i to certain fixed values. Then, for each fixed value of x we generate a pseudo-data point by assuming the data follows a normal distribution about the truth with uncertainty given by

$$\Delta g(x) = \frac{\alpha}{\sqrt{g(x)}}. \quad (2.2)$$

Here, the parameter α in Eq. (2.2) is used to scale the size of uncertainty. In the region where the magnitude of pseudo-PDF is small, the size of uncertainty is large, mimicking the case of real world data which has larger statistical uncertainty in regions where event numbers are small. We generate pseudo-data sets using

$$g_D(x) = \left(1 + r \times \Delta g(x)\right) g(x), \quad (2.3)$$

where the random variable r follows a Gaussian distribution with unit standard deviation. Although, it is possible to include correlated systematic uncertainties or even full likelihoods from experimental data, for simplicity, we treat the pseudo-PDF uncertainty to be uncorrelated and purely statistical.

¹ The use of a deep neural network is supported by the Universal Approximation Theorem [23] whereas a polynomial is supported by the Stone-Weierstrass Theorem [24, 25]. These theorems ensure that any smooth function can be well approximated either by neural networks or by polynomials.

For the following analysis, we create six pseudo-data sets that are summarized later in Table IV. In this section we describe only two of those pseudo-data sets, which have different underlying truth values and thus are in tension with each other. We refer to these two data sets as pseudo-data #1 and pseudo-data #2. These pseudo-data sets are generated on the same array of x values but with different values of parameters a_i as shown in Table I. The comparison of these two pseudo-data sets, along with that of their respective pseudo-PDF truths, is shown in Fig. 1. The tension between the pseudo-data sets is strong in the range $10^{-2} < x < 0.1$, and less significant in other ranges of x . Generating the pseudo-data sets for the same values of x ensures that the tension is explicit without any wiggle-room to smooth over tension with a flexible parameterization of pseudo-PDFs or due to a different theoretical model. It is important to note that, in general, inconsistencies in data might be a result of an inadequate theoretical model, such as underestimation of theoretical uncertainties or a less flexible parametrization of non-perturbative PDFs, or from an under-estimation of the experimental data error. In either case, the GMM method we propose here, will be able to capture uncertainties from both theoretical and experimental. Hence, we do not concern ourselves with the sources of data tension, but rather, we investigate methods to estimate uncertainty when fitting inconsistent data with a fixed theoretical prescription.

	N_{pt}	a_0	a_1	a_2	a_3	a_4	a_5
pseudo-data #1	50	30	0.5	2.4	4.3	2.4	-3.0
pseudo-data #2	50	30	0.5	2.4	4.3	2.6	-2.8

TABLE I. The choice of parameters (a_i) of the function $g(x)$ defined in Eq.(2.1) used to generate the two pseudo-data sets #1 and #2. N_{pt} refers to the number of data points in the set.

II.2. Least Squares Fits and Tension

Before introducing the GMM method we first illustrate the method of dealing with inconsistent data in the Least Squares fitting framework. Fits are performed by optimizing the log likelihood, which in our case is the χ^2 function defined as

$$\chi^2(\theta) = \sum_{j=1}^{N_{\text{pt}}} \left(\frac{y_i - T(\theta)}{\Delta y_i} \right)^2. \quad (2.4)$$

Given the known N_{pt} measurements y_i associated with uncertainties Δy_i , the χ^2 provides a normalized distance from theoretical predictions $T(\theta)$ to the measurements. Here θ are the fit parameters,

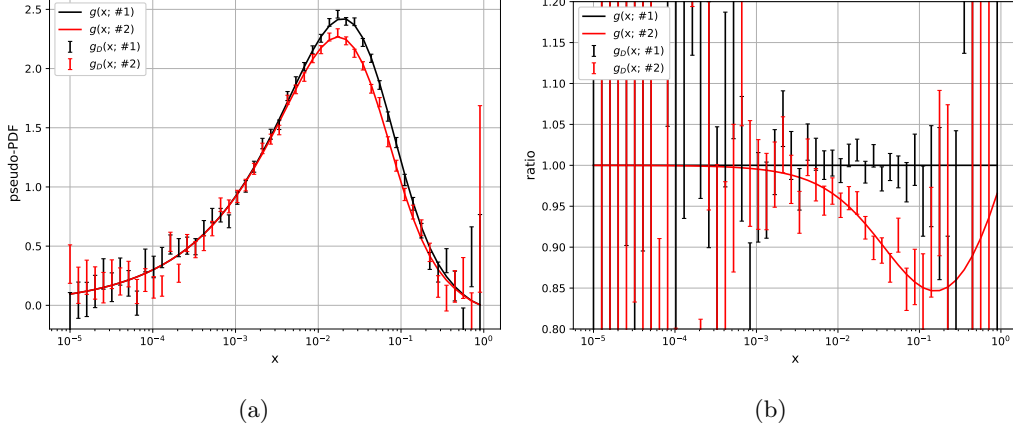


FIG. 1. Two pseudo-data sets, $g_D(x; \#1)$ (black) and $g_D(x; \#2)$ (red) are in tension with each other. The underlying truth $g(x)$ for individual pseudo-data sets are also shown by the solid curves which are referred to as truth $g(x; \#1)$ and truth $g(x; \#2)$. The plot on the left shows the pseudo-PDFs whereas the plot on the right shows their ratio with respect to the underlying truth $g(x; \#1)$.

which are some subset of the parameters a_i , and are varied in order to optimize the χ^2 function.

To illustrate the problem with the LS fit when tension exists, three parallel LS fits are performed, which we refer to as SG-A (performed only with pseudo-data #1), SG-B (performed only with pseudo-data #2) and SG-C (performed by combining both pseudo-data #1 and pseudo-data #2). We label these fits as ‘‘SG’’ to refer to the single-Gaussian nature of the likelihood in LS method, in contrast to the multi-modal distribution that we will introduce later. Results of these fits are shown in Table II. In these fits, we use the true functional form in Eq. (2.1), for the theory calculation, and fix parameters $\{a_0, a_1, a_2, a_3\}$ to their true values which can be found in Table I. The parameters a_4 and a_5 are varied and the values that minimize the χ^2 function are shown in Table II. The values of $\chi_{\#1}^2/N_{\text{pt}}$, $\chi_{\#2}^2/N_{\text{pt}}$, and $\chi_{\#1+\#2}^2/N_{\text{pt}}$ indicate the goodness of fit to individual pseudo-data sets # 1, # 2 and the combined pseudo-data set respectively. A good fit will have values of a $\chi^2/N_{\text{pt}} \sim 1$, whereas a poor fit has χ^2/N_{pt} values significantly larger than 1. The best-fit of SG-A, where only pseudo-data set # 1 is included, is found at the minimum of $\chi_{\#1}^2/N_{\text{pt}} = 0.88$, with values of $a_4 = 2.32$ and $a_5 = -3.22$. Also shown in the same row for SG-A are values of $\chi_{\#2}^2/N_{\text{pt}}$ and $\chi_{\#1+\#2}^2/N_{\text{pt}}$, these indicate the values of each of the likelihood functions $\chi_{\#2}^2/N_{\text{pt}}$ and $\chi_{\#1+\#2}^2/N_{\text{pt}}$ determined at the best fit values of a_4 and a_5 for fits SG-A. We see that for SG-A the values of $\chi_{\#2}^2/N_{\text{pt}} = 6.55$ and $\chi_{\#1+\#2}^2/N_{\text{pt}} = 3.72$ are significantly larger than one, indicating that there is significant tension between both the combined data set and the data set #2.

Likewise, the best-fit of SG-B, where only pseudo-data set # 2 is included, is found at the

minimum of $\chi_{\#2}^2/N_{\text{pt}} = 1.02$, indicating a reasonably good fit. For SG-B, the values $\chi_{\#1}^2/N_{\text{pt}}$ and $\chi_{\#1+\#2}^2/N_{\text{pt}}$ are determined by using the best fit value of $a_4 = 2.63$ and $a_5 = 2.72$. Once again large values of $\chi_{\#1}^2/N_{\text{pt}} = 7$ and $\chi_{\#1+\#2}^2/N_{\text{pt}} = 4.01$ indicate tension with both the combined data set and data set #1. Recall, that tension between the two data-sets, pseudo-data #1 and pseudo-data #2 are generated by starting with different choices of a_4 and a_5 as given in Table I. It can be seen, as expected, that the best-fit values of a_4 and a_5 in the two fits without tension, namely SG-A and SG-B, are indeed close to their underlying truth values.

The fit, SG-C, to the the combined data set where both pseudo-data sets # 1 and # 2 are included, is found at the minimum of $\chi_{\#1+\#2}^2/N_{\text{pt}} = 2.42$, indicating, as expected, a poor fit to the combined data set. In this case, the values of $\chi_{\#1}^2/N_{\text{pt}} = 2.27$, $\chi_{\#2}^2/N_{\text{pt}} = 2.42$ indicate that the combined fit, still has tension with both individual data sets.

fits	pseudo-data	N_{pt}	best-fit a_4	best-fit a_5	$\chi_{\#1}^2/N_{\text{pt}}$	$\chi_{\#2}^2/N_{\text{pt}}$	$\chi_{\#1+\#2}^2/N_{\text{pt}}$
SG-A	# 1	50	2.32	-3.22	0.88	6.55	3.72
SG-B	# 2	50	2.63	-2.73	7.00	1.02	4.01
SG-C	# 1 and # 2	100	2.48	-2.94	2.27	2.56	2.42
truth	# 1	-	2.4	-3.0	-	-	-
truth	# 2	-	2.6	-2.8	-	-	-

TABLE II. The table shows the best-fit values of a_4 and a_5 , as well as a measure of the goodness of fit χ^2/N_{pt} for three Least Square fits SG-A, SG-B, and SG-C, performed using pseudo-data sets # 1 and # 2. The columns $\chi_{\#1}^2/N_{\text{pt}}$, $\chi_{\#2}^2/N_{\text{pt}}$ and $\chi_{\#1+\#2}^2/N_{\text{pt}}$ indicate the values of these log-likelihood functions evaluated at values of a_4 and a_5 in the given rows. Also shown, for comparison, in the last two rows are the true values of a_4 and a_5 that were used to generate the two psuedo-data sets.

Although the fit to the combined data is poor, the main problem arises when attempting to determine the relevant uncertainty associated with such a fit. This is illustrated in Fig. 2, which presents Results of the LS fits SG-A, SG-B and SG-C. For all the three fits, results are presented in the form of replica sets, where the probability distribution of the pseudo-PDF is sampled with the Monte Carlo method as described in [6]. For the purpose of comparison, we also estimate the uncertainty of SG-C fit using the Hessian method [1], which is consistent with the Monte Carlo method. Here we only consider the Hessian uncertainty generated by the variation of χ^2 and determine the uncertainty with the criterion that $\Delta\chi^2 = 1$. Here, we do not include any additional tolerance criterion, such as the two-tier penalty for the CT uncertainty [1] and the dynamic tolerance

for the MSHT uncertainty [2]. Later, we will include such tolerance criteria for comparison with the GMM.

In panels 2(a) and 2(b), pseudo-PDFs from fits SG-A, SG-B and SG-C are found to be in disagreement in the range $10^{-3} < x < 0.2$. Even the 1σ uncertainty bands do not overlap in this region. For $x > 0.2$, the tension in data is weak due to larger uncertainty in the data and this can be seen from the overlap of the uncertainty bands in this region. Even though the uncertainty bands overlap at large x , the impact of significant tension in the range $10^{-3} < x < 0.2$ still affects pseudo-PDF at large x as can be observed by the different shapes of the uncertainty bands for the different LS fits. For the LS fit SG-C, the Hessian uncertainty with $\Delta\chi^2 = 1$ is also provided, which deviates from the Monte Carlo uncertainty by a negligible amount. The tension between the different fits, SG-A, SG-B and SG-C, can also be observed by looking at the result of the fits to the parameters a_4 and a_5 , shown in Fig. 2(c). As expected, the true values of the parameters a_4 and a_5 fall within the regions covered by the Monte Carlo sample of 1000 replicas for each of the fits SG-A and SG-B. However, the true values of the fit parameters are far from any of the replicas generated with SG-C. Furthermore, none of the replicas generated for either of the fits overlap and to make matters worse, neither the 1σ nor 3σ uncertainty bands of SG-C, generated using the Hessian method, overlap with the two truth values for a_4 and a_5 shown in Table I. The tolerance criteria used by the PDF fitting groups would increase the uncertainty, but as to be shown in Section IV, this approach will not be sufficient to incorporate both data sets into a single fit.

One might wonder why the fit SG-C, which combines both data sets, is unable to reproduce the desired uncertainty bands that should look like some combination of the uncertainty bands of both SG-A and SG-B. Such a combination of uncertainty bands would arise only if the likelihood function were multi-modal. On the other hand, fit SG-C assumes that there is only a single mode for the likelihood. In other words, we have ignored the two individual likelihoods generated by the two data sets and tried to define a new likelihood in SG-C that we have assumed to be uni-modal. Another way of stating this is to say that a naive combination of Monte-Carlo samples from SG-A and SG-B, seen in Fig. 2(c), is a better representation of the combined likelihood of both data sets. This combined likelihood is multi-modal, unlike that of SG-C. Of course, just by adding the Monte Carlo samples does not suffice and we need a proper method to combine the samples. In order to combine likelihoods in a statistically robust way, we introduce the GMM method in the next section which provides a way to combine likelihoods into a multi-modal distribution.

Before we conclude this section, we comment on alternate methods to deal with such incon-

sistencies in fits. For example, the Particle Data Group (PDG) [26], recommends increasing the uncertainty on data sets, either all data sets if they are of similar precision or the data set from the experiment with the highest precision, by a scale factor $S = \sqrt{\chi^2/N_{\text{pt}}}$. For data sets with tension, $\sqrt{\chi^2/N_{\text{pt}}} > 1$ and hence the scale factor $S > 1$, implying an increase in uncertainty. For a large data set ($N_{\text{pt}} \gg 1$), increasing the uncertainty on all data sets implies that $\chi^2/N_{\text{pt}} \simeq 1$, thus ensuring a good fit. This idea has been further explored and elucidated in both the Bayesian and Frequentist approach [27–29]. The GMM presented here, not only provides an alternate way to combine inconsistent data sets without increasing their uncertainty, but also, if desired, provides an alternate estimate for the scale factor S required to make data sets consistent. We describe some of these ideas briefly in Sec. V.2.

III. GAUSSIAN MIXTURE MODEL IN PDF FIT

As mentioned in the earlier section, the likelihood from each of the data sets (pseudo-data #1 and pseudo-data #2) are significantly different and needs to be combined in a meaningful way. We propose the use of the Gaussian Mixture Model to construct the combined likelihood for data with tension.

The GMM was first used by Karl Pearson in 1894 [30]. It is now used extensively as an unsupervised machine learning technique to classify data [31]. In general, the GMM is a mixture of K base Gaussian distributions. Given the data set $Y = \{(y_1, \Delta y_1), (y_2, \Delta y_2), \dots, (y_{N_{\text{pt}}}, \Delta y_{N_{\text{pt}}})\}$, where Δy_j is the uncertainty associated with the measured value y_j ², we can define the GMM likelihood as

$$L(Y|\vec{\theta}) = \prod_{j=1}^{N_{\text{pt}}} \pi(y_j, \Delta y_j|\vec{\theta}) = \prod_{j=1}^{N_{\text{pt}}} \sum_{i=1}^K \omega_i \mathcal{N}(y_j, \Delta y_j|\theta_i), \quad (3.1)$$

$$0 \leq \omega_i \leq 1 \quad \text{and} \quad \sum_i \omega_i = 1,$$

where the i 'th base distribution $\mathcal{N}(y_j, \Delta y_j|\theta_i)$ is associated with a normalized weight ω_i . Here θ_i corresponds to the fit parameters. For example, for the fits performed in the previous section $\theta_i = \{a_{4_i}, a_{5_i}\}$ where $i = 1, 2, \dots, K$. Therefore, performing a two parameter fit with K Gaussians, requires $2 \times K$ parameters. To simplify the following expressions, we will abbreviate \mathcal{N} and π for

² For clarity of presentation, we use an uncorrelated data set and present formulas for this scenario. These can easily be generalized when correlated uncertainties are present.

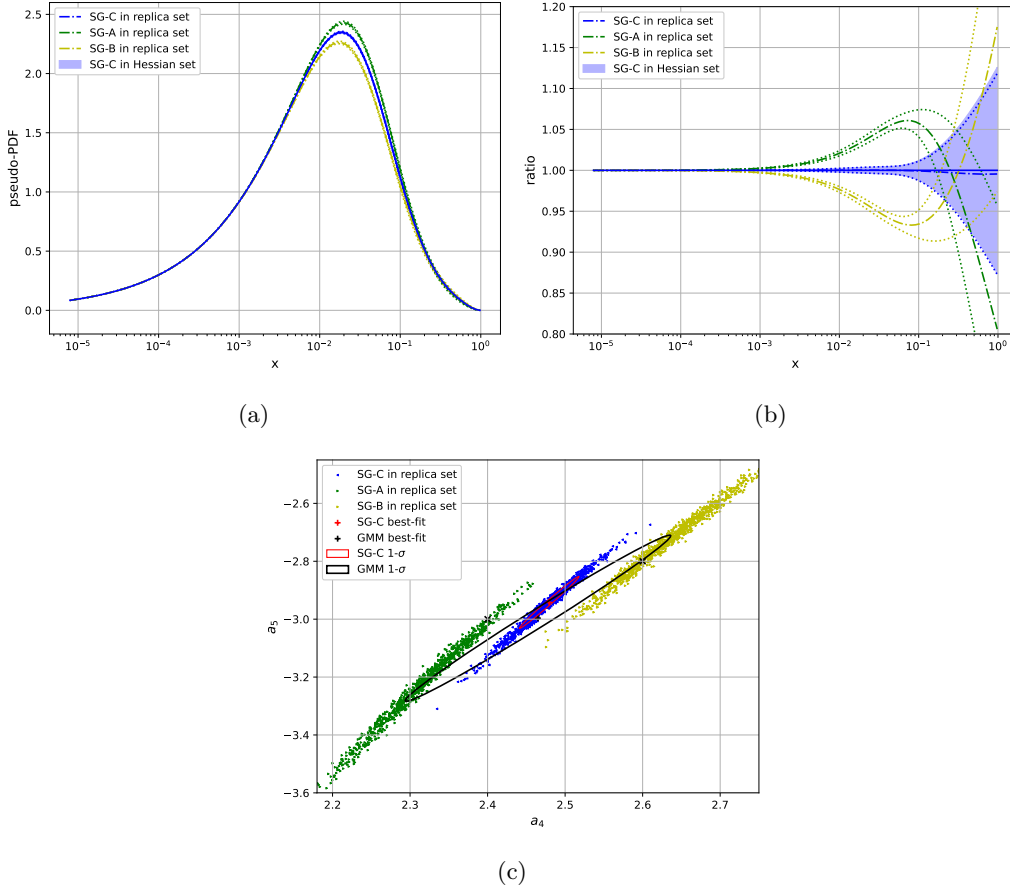


FIG. 2. Panel (a): the comparison of pseudo-data and optimal pseudo-PDFs. The uncertainties in replica sets correspond to the 1 standard deviation interval. For the LS fit C , the Hessian uncertainty with $\Delta\chi^2 = 1$ is also provided, which deviates from the Monte Carlo uncertainty by a negligible amount. The sizes of uncertainties are small in view of the magnitudes of pseudo-PDFs. Panel (b): similar to panel (a), but for ratios to the central value of the Hessian set of the SG-C fit. Panel (c): clouds of fitted values of parameters a_4 and a_5 in replica sets, as compared to true values.

the i 'th base distribution and the j 'th measurement as follows

$$\mathcal{N}(y_j, \Delta y_j | \theta_i) = \mathcal{N}_{ij}, \quad \pi(y_j, \Delta y_j | \vec{\theta}) = \pi_j. \quad (3.2)$$

Notice that the number of original parameters N_{param} has increased in the GMM by a factor K . This means that we need to determine not only the central value of $K \times N_{\text{param}}$ parameters but also the uncertainty on each of them. Later we will describe how this fit to $K \times N_{\text{param}}$ parameters can be combined in a meaningful way to produced a fit and uncertainty on only N_{param} parameters.³ In

³ For example, there were two fit parameters (a_4 and a_5) in the LS fits in Sec. II, whereas in the GMM there would be $2 \times K$ parameters. Ultimately, we want to be able determine the uncertainty on two parameters and not $2 \times K$ parameters.

the GMM, the logarithm of the likelihood function is

$$\begin{aligned}
 -\ln L &= -\ln \left(\prod_{j=1}^{N_{\text{pt}}} L(y_j, \Delta y_j | \vec{\theta}) \right) = -\sum_{j=1}^{N_{\text{pt}}} \ln \left(\sum_{i=1}^K \omega_i \mathcal{N}_{ij} \right) \\
 &= -\sum_{j=1}^{N_{\text{pt}}} \ln \left(\sum_{i=1}^K \frac{\omega_i}{\sqrt{2\pi}\Delta y_j} \exp \left[-\frac{1}{2} \left(\frac{y_j - T(\theta_i)}{\Delta y_j} \right)^2 \right] \right). \tag{3.3}
 \end{aligned}$$

For a single Gaussian distribution with $K = 1$, the log-likelihood in Eq. (3.3) is proportional to χ^2 , which reproduces the Least Square method as shown in the equation below

$$-\ln L = -\sum_{j=1}^{N_{\text{pt}}} \ln \left(\mathcal{N}(y_j, \Delta y_j | \theta) \right) = \frac{1}{2} \chi^2 + \sum_{j=1}^{N_{\text{pt}}} \ln \left(\sqrt{2\pi} \Delta y_j \right). \tag{3.4}$$

Notice, in Eq. (3.3), we have chosen to define the likelihood, such that each Gaussian has information about all experimental data points, i.e. for each Gaussian we sum over all values of $j = 1$ to $j = N_{\text{pt}}$. An alternate way of defining the likelihood would be to distribute the experimental data among the various Gaussians, i.e. each data set would have its own Gaussian. These two definitions have different interpretations. In the latter, we are trying to assign different theoretical predictions to different experiments, whereas in the former we are trying to find the theoretical values that different combinations of all experiments predict. Since we are trying to combine all experiments into a single global fit, we focus on using the definition as given in Eq. (3.3).

The GMM method allows us to extend the statistical model assumed in the optimization procedure, from a single Gaussian distribution to a more generalized configuration, where a multi-modal feature is allowed. Importantly, for a consistent data set we will see that the multiple Gaussian modes will overlap and yield a result that is equivalent to a single Gaussian, i.e. the Least Squares fit. We will discuss the consistency between the GMM and LS methods in Sec. V.

III.1. Performing parameter fits with the GMM

In order to determine the best fit parameters, we minimize the the log-likelihood defined in Eq. (3.3). We remark here that, conventinally the Expectation Maximization algorithm [31] is used to learn the best fit parameters of the mixture model.⁴ The advantage of this algorithm is that it provides an iterative method that does not require information about the derivative of the likelihood. However, in our setup, a straightforward implementation of the Expectation

⁴ We remark here that it is possible to use the Expectation Maximization algorithm if we produce a large pseudo-data set and apply the Gaussian mixture model directly to the theory parameter space.

Maximization algorithm is not possible since we are trying to fit a nonlinear function. For the purpose of demonstration, we use methods that rely on information about the derivative of the likelihood. Specifically, we use `TensorFlow` [32] to determine derivatives of the likelihood and minimize the log-likelihood. As described in the previous section, the number of parameters have increased and for K Gaussians we have

$$N_{\text{param}}^{\text{GMM}} = K \times N_{\text{param}} + K - 1, \quad (3.5)$$

where, the last two terms, $K - 1$, come from the constraint on the weights ω_i that are required to sum to unity. We carry out minimization of the likelihood by varying all $N_{\text{param}}^{\text{GMM}}$ parameters.⁵ The gradient of the log-likelihood with respect to the fit parameters that belong to i -th Gaussian is

$$\frac{\partial}{\partial \theta_i} \ln L = \sum_{j=1}^{N_{\text{pt}}} \omega_i \frac{\mathcal{N}_{ij}}{\pi_j} \frac{y_j - T(\theta_i)}{\Delta y_j^2} \frac{\partial T(\theta_i)}{\partial \theta_i}, \quad (3.6)$$

and that with respect to weight ω_i is

$$\frac{\partial}{\partial \omega_i} \ln L = \sum_{j=1}^{N_{\text{pt}}} \frac{\mathcal{N}_{ij}}{(\sum_{i=1}^K \omega_i \mathcal{N}_{ij})} = \sum_{j=1}^{N_{\text{pt}}} \frac{\mathcal{N}_{ij}}{\pi_j}. \quad (3.7)$$

Optimal values, $\hat{\theta}_i$, for the parameters θ_i are found by extremizing the log-likelihood by solving [33]

$$\left. \frac{\partial}{\partial \theta_i} \ln L \right|_{\theta_i = \hat{\theta}_i} = 0 \quad (3.8)$$

along with a similar equation involving the weights ω_i ,

$$\left. \frac{\partial}{\partial \omega_i} \ln L \right|_{\omega_i = \hat{\omega}_i} = 0. \quad (3.9)$$

In this work, we extremize the log-likelihood function by using the `Adam` optimizer with learning rate being 10^{-6} provided by the `TensorFlow` API [32]. Note that, in Eq. (3.6), the best-fit value of the prediction $y_j(\theta_i)$ is weighted not only by the variance in measurements (Δy_i), but also by the weights ω_i and the factor $\mathcal{N}(y_j|\theta_i)/\pi(y_j, \Delta y_j|\vec{\theta})$ of the i -the base distribution, which becomes trivial for a single Gaussian. The Jacobian $\partial y_j(\theta_i)/\partial \theta_i$, transforms information from the data space to the PDF space. The presence of this transformation makes it difficult to use the Expectation Maximum algorithm.

⁵ It is possible to determine the value of the weights ω_i in other more complicated ways since they indicate the degree of importance to each Gaussian. Here we take the approach that we learn the values of ω_i directly from the data and hence it is also varied during the minimization process.

In this work we use the above equation as a constraint that determines the value of ω_i . This is generally the approach taken for other unsupervised machine learning applications. In general, this strategy tends to assign higher weights to experiments with higher precision. If desired, it is possible to control the weights by increasing or decreasing the value of the uncertainties associated with a certain experimental data set.⁶ Thus along with θ_i , the weights ω_i are also varied in order to optimize the log-likelihood.

III.2. Mean and Uncertainty in the GMM

It is straightforward to show that the expectation value of parameters is the weighted sum of the optimal parameters for individual base distributions,

$$\mathbb{E}[\theta] = \sum_{i=1}^K \omega_i \hat{\theta}_i. \quad (3.10)$$

Consequently, an experiment with higher precision would be associated with a higher weight and, as a result, the central value of the parameters is pulled towards those values that better agree with higher precision experiments.

There are several ways to determine the uncertainty with the modified log-likelihood. Below, we describe the use of the observed Fisher Information Matrix to estimate uncertainty [33] on the fit parameters. We note that this is only one way to estimate the uncertainty and there are other possible methods which will be discussed in detail elsewhere.

For the case of single Gaussian or when all the Gaussians have the same mean and covariance, the observed Fisher information matrix reduces to the usual Hessian matrix used to determine the covariance of the fit parameters in the LS method.⁷ Like the Hessian matrix, the information matrix can also be found with numerical methods. Here we use algorithmic differentiation [34] within `TensorFlow` to determine derivatives of the likelihood function. We note that the information matrix is only an estimate of the covariance of the GMM and it is possible to determine the covariance matrix as well, which will be described in detail elsewhere.

⁶ One method of trying to deal with inconsistent data sets is to artificially inflate uncertainties until we arrive at a consistent data set [16]. Although not described in this work, we remark that the GMM in conjunction with certain information criteria, provides a way to determine the extent to which it is necessary to inflate the uncertainty on data until the fits become consistent.

⁷ For the GMM with multiple Gaussians, the likelihood function as defined in Eq. (3.3) includes all experimental points for each Gaussian. Thus, if the means of each Gaussian are identical, then this implies that the covariance, which is related to the second order derivative about the minimum of the likelihood, must also be identical, c.f. Eq. (3.18). In general, the covariance matrices for Gaussians with identical means may be different in the GMM if the likelihoods were to be defined differently.

Elements of the information matrix (\mathcal{I}) are determined by taking a further derivative on Eq. (3.8) as follows,

$$\begin{aligned} (\mathcal{I})_{mk} &= -\frac{\partial^2}{\partial\theta_m\partial\theta_k} \ln L = \frac{\partial}{\partial\theta_m} \left(-\sum_{j=1}^{N_{\text{pt}}} \frac{\omega_k}{\pi_j} \frac{\partial\mathcal{N}_{kj}}{\partial\theta_k} \right) \\ &= \sum_{j=1}^{N_{\text{pt}}} \left[-\frac{\omega_k}{\pi_j} \frac{\partial^2\mathcal{N}_{mj}}{\partial\theta_m\partial\theta_m} \delta_{mk} + \frac{\omega_k\omega_m}{\pi_j^2} \frac{\partial\mathcal{N}_{mj}}{\partial\theta_m} \frac{\partial\mathcal{N}_{kj}}{\partial\theta_k} \right] \end{aligned} \quad (3.11)$$

Notice that for a fit with N_{param} parameters per Gaussian, the information matrix is a $(KN_{\text{param}}) \times (KN_{\text{param}})$ symmetric matrix, i.e. it spans a space that is a direct product of an N_{param} parameter and a K parameter space. The second term contributes to the elements of the information matrix (\mathcal{I}) that are off-diagonal in K -space but not in N_{param} space. In contrast, the off-diagonal terms in N_{param} space contribute to the covariance matrix. On the other hand, the K -space off-diagonal terms are small since they must add up to the left hand side of Eq. (3.8), which vanishes at $\theta_i = \hat{\theta}_i$ by definition. This is also verified numerically for all of the fits performed here. For simplicity, we will neglect these particular K -space off-diagonal terms and only consider the $N_{\text{param}} \times N_{\text{param}}$ block diagonal terms of the information matrix. Although, it is not necessary to neglect these off diagonal terms, this allows us to quickly approximate the probability distribution function in parameter space (θ) as a mixture of Gaussians. In other words, we are trying to use the Likelihood function defined in Eq. (3.3), to approximate the probability distribution function of θ . Thus, we assume that, when evaluated at the mean ($\theta_i = \hat{\theta}_i$) the information matrix takes on an approximate block diagonal form, with each $N_{\text{param}} \times N_{\text{param}}$ block belonging to the subspace of the i 'th Gaussian $\mathcal{N}(y_j, \Delta y_j | \theta_i)$. We denote the information matrix for individual base distributions of the GMM as $\mathcal{I}_{\text{GMM},i} = -(\partial^2 \ln L / \partial\theta_i \partial\theta_i) / \omega_i$, which are the unweighted $N_{\text{param}} \times N_{\text{param}}$ diagonal blocks of the full information matrix \mathcal{I} . An estimate of the covariance of individual base Gaussian distributions of the GMM is then,

$$\text{cov}_{\text{GMM},i} \simeq \left(\mathcal{I}_{\text{GMM},i} \right)^{-1} = \left(\sum_{j=1}^{N_{\text{pt}}} \left[-\frac{1}{\pi_j} \frac{\partial^2\mathcal{N}_{ij}}{\partial\theta_i^2} + \frac{\omega_i}{\pi_j^2} \left(\frac{\partial\mathcal{N}_{ij}}{\partial\theta_i} \right)^2 \right] \right)^{-1} \quad (3.12)$$

We can now define the probability distribution of the parameters of the fit as mixture of Gaussians as follows:

$$\begin{aligned} \mathcal{P}(x | \theta_i, \text{cov}_{\text{GMM},i}) &= \sum_{i=1}^K \frac{\omega_i}{(2\pi)^{N_{\text{param}}/2} \det(\text{cov}_{\text{GMM},i})^{1/2}} \\ &\times \exp \left[-\frac{1}{2} \left((x - \theta_i)^T \cdot (\text{cov}_{\text{GMM},i})^{-1} \cdot (x - \theta_i) \right) \right]. \end{aligned} \quad (3.13)$$

With this definition, we can now determine estimates of the uncertainty on the parameters θ . We first note that when $K = 1$, we have a single Gaussian and Eq. (3.11) reduces to the Hessian matrix of the LS method,

$$-\frac{\partial^2}{\partial\theta\partial\theta}\ln L\Big|_{\theta=\hat{\theta}} = \frac{1}{2}\frac{\partial^2}{\partial\theta\partial\theta}\chi^2\Big|_{\theta=\hat{\theta}} = \sum_{j=1}^{N_{\text{pt}}}\frac{1}{\Delta y_j^2}\frac{\partial^2 T(\theta)}{\partial\theta^2}\Big|_{\theta=\hat{\theta}}, \quad (3.14)$$

and the covariance is

$$\text{cov}_{\chi^2} = \left(\sum_{j=1}^{N_{\text{pt}}}\frac{1}{\Delta y_j^2}\frac{\partial^2 T(\theta)}{\partial\theta^2}\Big|_{\theta=\hat{\theta}} \right)^{-1}. \quad (3.15)$$

For the GMM, in order to provide a useful estimate of uncertainty, we need to reduce the $(KN_{\text{param}}) \times (KN_{\text{param}})$ space to a $(N_{\text{param}}) \times (N_{\text{param}})$ space in a meaningful way. To that end, let us consider the covariance of the GMM which is defined as

$$\begin{aligned} \text{cov}_{\text{GMM}} &= \mathbb{E}[\theta^2] - \mathbb{E}[\theta]^2 \\ &= \sum_{i=1}^K \omega_i \hat{\theta}_i^{(2)} - \left(\sum_{i=1}^K \omega_i \hat{\theta}_i \right)^2, \end{aligned} \quad (3.16)$$

where $\hat{\theta}_i^{(2)}$ denotes the estimated second moment of parameters for the i -th base distribution. It can be re-expressed using the covariance of i -th base Gaussian distribution,

$$\hat{\theta}_i^{(2)} = \text{cov}_{\text{GMM},i} + \hat{\theta}_i^2. \quad (3.17)$$

Combining Eqs. (3.16) and (3.17), an estimate of the covariance of the GMM is given by

$$\begin{aligned} \text{cov}_{\text{GMM}} &= \sum_{i=1}^K \omega_i \text{cov}_{\text{GMM},i} + \sum_{i=1}^K \omega_i (\mathbb{E}[\theta] - \hat{\theta}_i)^2 \\ &\simeq \sum_{i=1}^K \omega_i \left(\sum_{j=1}^{N_{\text{pt}}} \left[-\frac{1}{\pi_j} \frac{\partial^2 \mathcal{N}_{ij}}{\partial\theta_i^2} + \frac{\omega_i}{\pi_j^2} \left(\frac{\partial \mathcal{N}_{ij}}{\partial\theta_i} \right)^2 \right] \right)^{-1} + \sum_{i=1}^K \omega_i (\mathbb{E}[\theta] - \hat{\theta}_i)^2. \end{aligned} \quad (3.18)$$

The covariance of the GMM shown in the above equation receives two contributions: the first is the weighted sum of covariances for the individual base distributions, and the second term accounts for differences in the mean values of each of the base distributions. When the means of each Gaussian overlap, the second term vanishes and the first term reproduces the covariance in LS method, Eq. (3.15).

IV. APPLICATION OF THE GMM IN A TOY MODEL OF PDFS

In this section, we compare results obtained by the GMM method, defined in Eq. (3.3), to those obtained using the LS method. When estimating uncertainty using the LS method, we first

diagonalize the Hessian and determine eigenvalue directions. We then determine values of the parameters that satisfy the $\Delta\chi^2 = 1$ condition and define the uncertainty on the fit parameters, which corresponds to the 68% confidence level interval. Here, we also implement the CT [1] and MSHT [2] tolerance criteria, which provide a more conservative estimate of uncertainty under the potential imperfections of fits. The comparison is presented in three cases of pseudo-data, including the two pseudo-data sets introduced in Sec. II.1.

IV.1. Applying GMM to different scenarios

In this section we consider three cases. In each case we combine certain pseudo-data sets. We list and describe each of these cases below:

- Case-1: Here we use pseudo-data sets # 1 and # 2 which were introduced in Sec. II.1. This case represents the scenario when there is strong tension between data sets. With this case, we will demonstrate how the GMM can provide an estimate of uncertainty in a statistically robust way.
- Case-2: Here we combine pseudo-data sets # 3 and # 4. The central values used to generate these data sets are the same as those used in # 1 and # 2, however, their uncertainties are tripled by increasing the value of α in Eq. (2.2) by a factor of three, as shown in Table III. The central values of data sets # 1 and # 3 as well as # 2 and # 4 do not overlap, because different random numbers (r), cf. Eq. (2.3), are used to generate them. With this combination we will be able to show how the GMM behaves when the errors of the data sets are large enough so that there is no tension. We can connect this to the alternative suggestions of dealing with uncertain data by artificially increasing the errors of the data sets [16].
- Case-3: This case contains pseudo-data sets # 5 and # 6. The tension in this case is generated only via variation of the parameter a_2 . The parameter a_2 controls the behaviour of the pseudo-PDF in the large- x region, where the uncertainty is large. We fit this case with parameters a_2 and a_4 . With this combination we demonstrate overfitting with the GMM method, and later in Sec. V.2 we will demonstrate how to deal with overfitting.

The true values of the parameters for cases 1 through 3 are presented in Table III and Fig. 3.

The best-fit obtained by the GMM method for the Case-1 is shown in Figs. 4(a) and 4(b) and Table IV. For the GMM likelihood function, we choose to fit with a mixture of two Gaussian

case	pseudo-data	α	N_{pt}	a_0	a_1	a_2	a_3	a_4	a_5
Case-1	#1	0.05	50	30	0.5	2.4	4.3	2.4	-3.0
	#2	0.05	50	30	0.5	2.4	4.3	2.6	-2.8
Case-2	#3	0.15	50	30	0.5	2.4	4.3	2.4	-3.0
	#4	0.15	50	30	0.5	2.4	4.3	2.6	-2.8
Case-3	#5	0.05	50	30	0.5	2.4	4.3	2.4	-3.0
	#6	0.05	50	30	0.5	1.4	4.3	2.4	-3.0

TABLE III. Similar to Table I, the summary of true values of the pseudo-PDF parameters and values of α in Eq. (2.2) for three cases. For comparison, we also include the true values of the pseudo-PDF parameters for Case-1 in this table.

distributions. As a result, the mean values of each Gaussian, can describe the two distinct pseudo-data sets well and in fact are very similar to what we obtain for SG-A and SG-B. We find the weights ω_i to be roughly equal, which is a result of the errors in each of the data sets #1 and #2 being almost equal and also having the same number of data points. In Figs. 4(c) and 4(d), the pseudo-PDF uncertainty estimated by the GMM is compared to uncertainties predicted using the LS method. For $10^{-3} < x < 0.1$, the (small) error band of SG-C pseudo-PDF exclude those of SG-A and SG-B fits, the error band estimated by the GMM is consistent and includes areas covered by both SG-A and SG-B pseudo-PDFs. For $x > 0.1$, where the error in the data sets are large, uncertainties from SG-C and the GMM overlap. Fig. 4(e) shows the results of the different fits in the fit parameter space. The $1-\sigma$ correlation ellipse estimated by SG-C is small, as has been mentioned before, and does not overlap with SG-A and SG-B replicas. On the other hand, the GMM correlation ellipse is large enough and, importantly, also possesses a different axes orientations, that enables the GMM covariance to overlap with some of the replicas of both SG-A and SG-B. Note, that we have represented the GMM by a single covariance matrix but this should not be confused with the covariance arising from a single Gaussian, since the shape of the GMM likelihood is multi-modal and not uni-modal.

For Case-2, shown in Fig. 5, the tension in the data set has been reduced by increasing the error on the data, so that SG-C describes the combined pseudo-data set with $\chi^2_{\#3+\#4}/N_{\text{pt}} = 1.04$. Even for such a mild tension, the fits SG-A and SG-B do not overlap with SG-C. On the other hand, the GMM fit overlaps with both SG-A and SG-B. The difference between the axes orientations of the correlation ellipses between SG-C and the GMM is small. Although, the GMM method

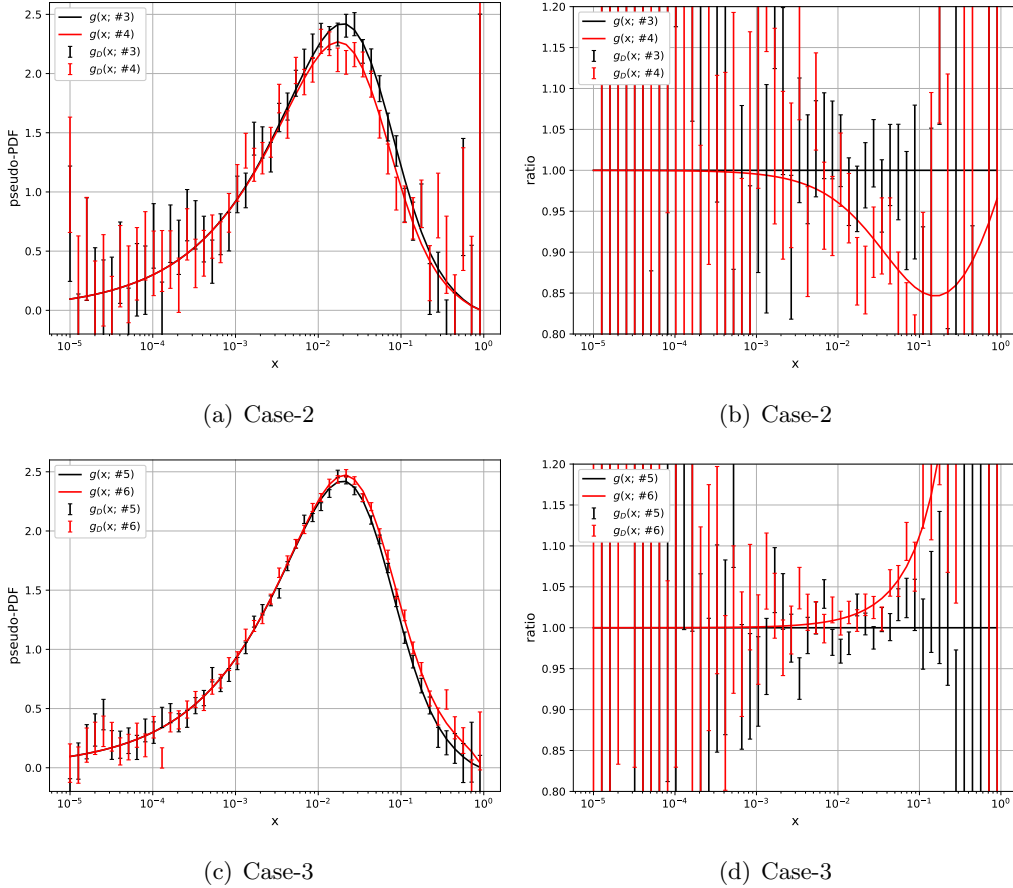


FIG. 3. Similar to Fig. 1, but for Case-2 and Case-3.

produces a larger uncertainty which is more consistent with SG-A and SG-B, the differences with SG-C are small and we need a way to determine whether we should stick with SG-C or with the GMM method. We will return to a discussion of this in Sec. V.2.

The performances for Case-3 of the GMM and LS methods are similar to Case-1. The LS method cannot fit both pseudo-data sets # 5 and # 6 well, c.f. the bottom rows of Table IV, even though the uncertainties in both data sets are large. The GMM is able to learn about the tension in these data sets and shows a strong inclination to two modes. In terms of the fitted pseudo-PDFs, the GMM in Fig. 6 systematically enlarges the uncertainty and envelopes both data sets # 5 and # 6 simultaneously.

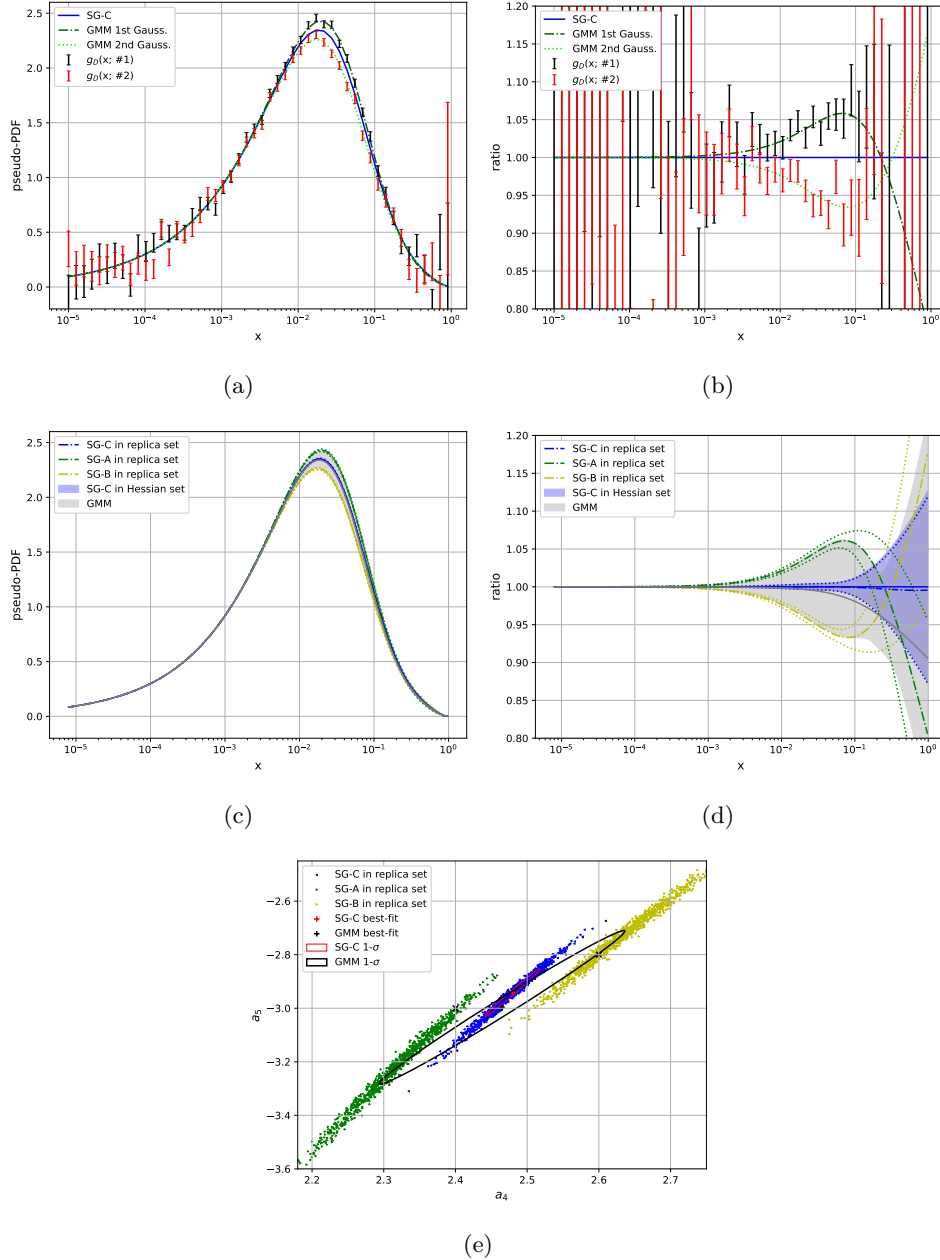


FIG. 4. Pseudo-PDFs obtained by the GMM method and the LS method for Case-1 are compared. Panel (a): The pseudo-data sets are compared to best-fit pseudo-PDFs. Although shown separately, the two best-fit pseudo-PDFs from the GMM method are eventually combined according to weights shown in Table IV. Panel (b): Similar to panel (a), but presented as ratios of the best-fit obtained from the SG-C fit. Panel (c): The absolute values of pseudo-PDFs for all SG-A, -B, -C, and GMM fits. Panel (d): Similar to panel (c), but presented as ratios to the best-fit obtained from the SG-C Hessian set. Panel (e): The correlation ellipse from the GMM method is compared to SG-C correlation ellipses, and to replicas from SG-A, -B, and -C fits. The best-fit points are located at their corresponding values in Table IV, while the GMM best-fit corresponds to the weighted average of best-fit of two individual Gaussian distributions as given by Eq. (3.10).

Case-1	fits	pseudo-data	a_4	a_5	$\chi^2_{\#1}/N_{\text{pt}}$	$\chi^2_{\#2}/N_{\text{pt}}$	$\chi^2_{\#1+\#2}/N_{\text{pt}}$	weight
	SG-A	# 1	2.32	-3.22	0.88	6.55	3.72	-
	SG-B	# 2	2.63	-2.73	7.00	1.02	4.01	-
	SG-C	# 1 and # 2	2.48	-2.94	2.27	2.56	2.42	-
	GMM Gauss.-1	# 1 and # 2	2.31	-3.25	0.88	6.55	3.72	0.52
	GMM Gauss.-2	# 1 and # 2	2.64	-2.72	7.00	1.02	4.01	0.48
Case-2	fits	pseudo-data	a_4	a_5	$\chi^2_{\#3}/N_{\text{pt}}$	$\chi^2_{\#4}/N_{\text{pt}}$	$\chi^2_{\#3+\#4}/N_{\text{pt}}$	weight
	SG-A	# 3	2.20	-3.50	0.76	1.68	1.22	-
	SG-B	# 4	2.74	-2.54	1.61	0.89	1.25	-
	SG-C	# 3 and # 4	2.48	-2.98	0.96	1.11	1.04	-
	GMM Gauss.-1	# 3 and # 4	2.40	-3.10	0.81	1.36	1.09	0.69
	GMM Gauss.-2	# 3 and # 4	2.66	-2.73	1.68	0.90	1.29	0.31
Case-3	fits	pseudo-data	a_2	a_4	$\chi^2_{\#5}/N_{\text{pt}}$	$\chi^2_{\#6}/N_{\text{pt}}$	$\chi^2_{\#5+\#6}/N_{\text{pt}}$	weight
	SG-A	# 5	2.27	2.40	1.16	2.33	1.75	-
	SG-B	# 6	1.25	2.41	2.46	0.82	1.64	-
	SG-C	# 5 and # 6	1.60	2.41	1.54	1.14	1.34	-
	GMM Gauss.-1	# 5 and # 6	2.06	2.40	1.19	1.96	1.58	0.58
	GMM Gauss.-2	# 5 and # 6	1.13	2.41	2.58	0.82	1.70	0.42

TABLE IV. The best-fit values of parameters, and χ^2/N_{pt} values for individual and combined pseudo-data sets obtained by the LS method and the GMM fit.

IV.2. The GMM method compared to different tolerance criteria

Estimations of PDF uncertainties are needed for inference from QCD experiments at the LHC and other facilities. Various factors that determine the accuracy of PDFs include the theoretical uncertainty, the insufficiently understood source of uncertainty due to the prescription for experimental systematic errors, the tension between experimental data, and the sampling of PDF functional forms and fitting methodologies, as detailed in Ref. [35]. Global PDF analysis groups are aware of the shortcomings of using a fixed tolerance $\Delta\chi^2 = 1$ and have proposed alternate methods. Specifically, CTEQ-TEA [1] and MSHT [2] global PDF analyses, both adopt certain tolerance criteria, known as the two-tier tolerance and the dynamic tolerance criteria, respectively, on top of the basic Hessian method.

In Sec. IV.1, we compared results of the GMM with the usual LS method of determining 1-

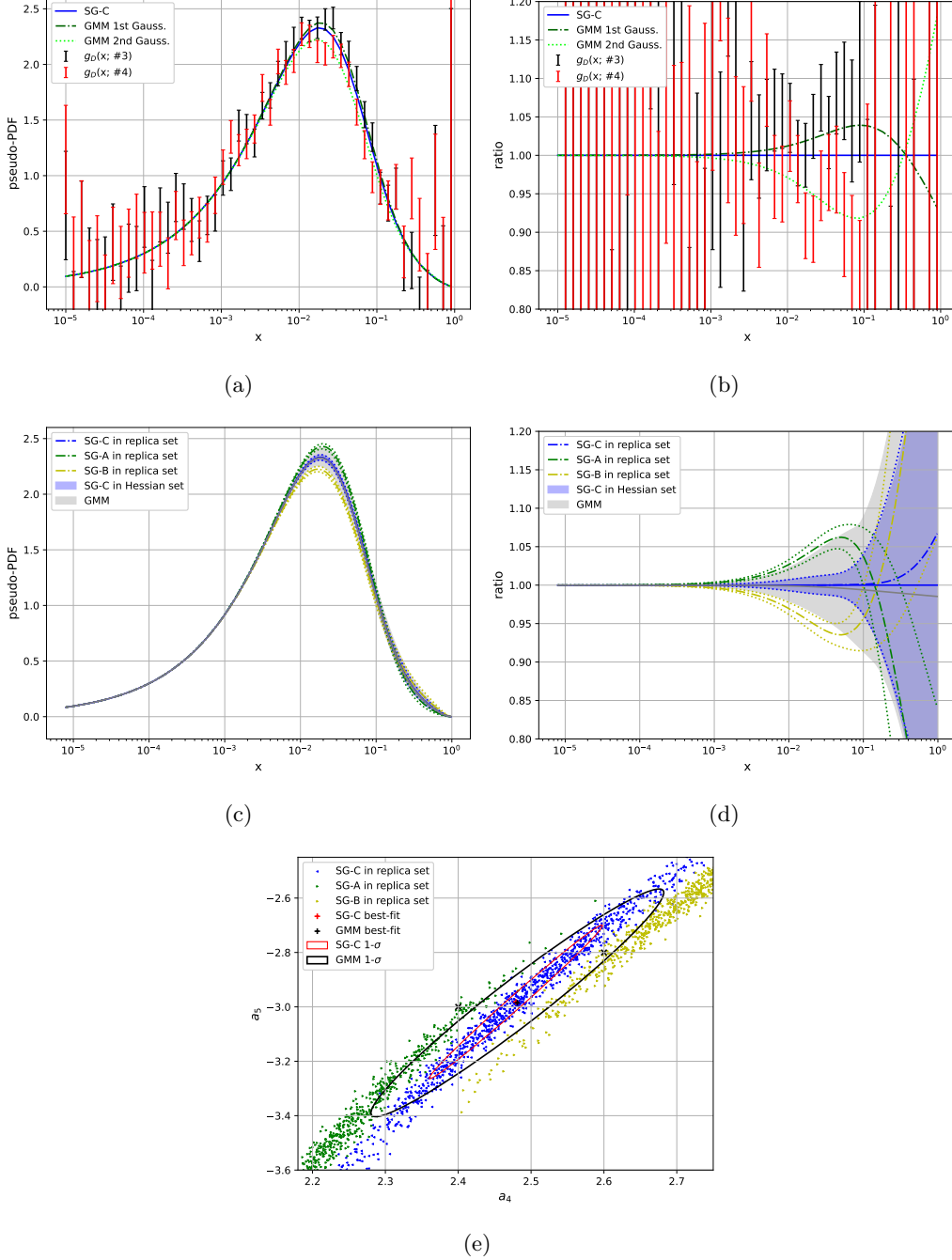


FIG. 5. Similar to Fig. 4, but for the Case-2.

σ contours by setting $\Delta\chi^2 = 1$. In this subsection, we compare the GMM results presented in Sec. IV.1 to the Hessian results with the CT and MSHT tolerance criteria.

We remind the reader that CTEQ-TEA Hessian eigenvector PDFs are constructed using a two-tier prescription [36, 37] that prevents unexpectedly large increments to either the global χ^2 or to the χ^2_E values of individual experiments. Hence, the CT PDF error sets are determined using a

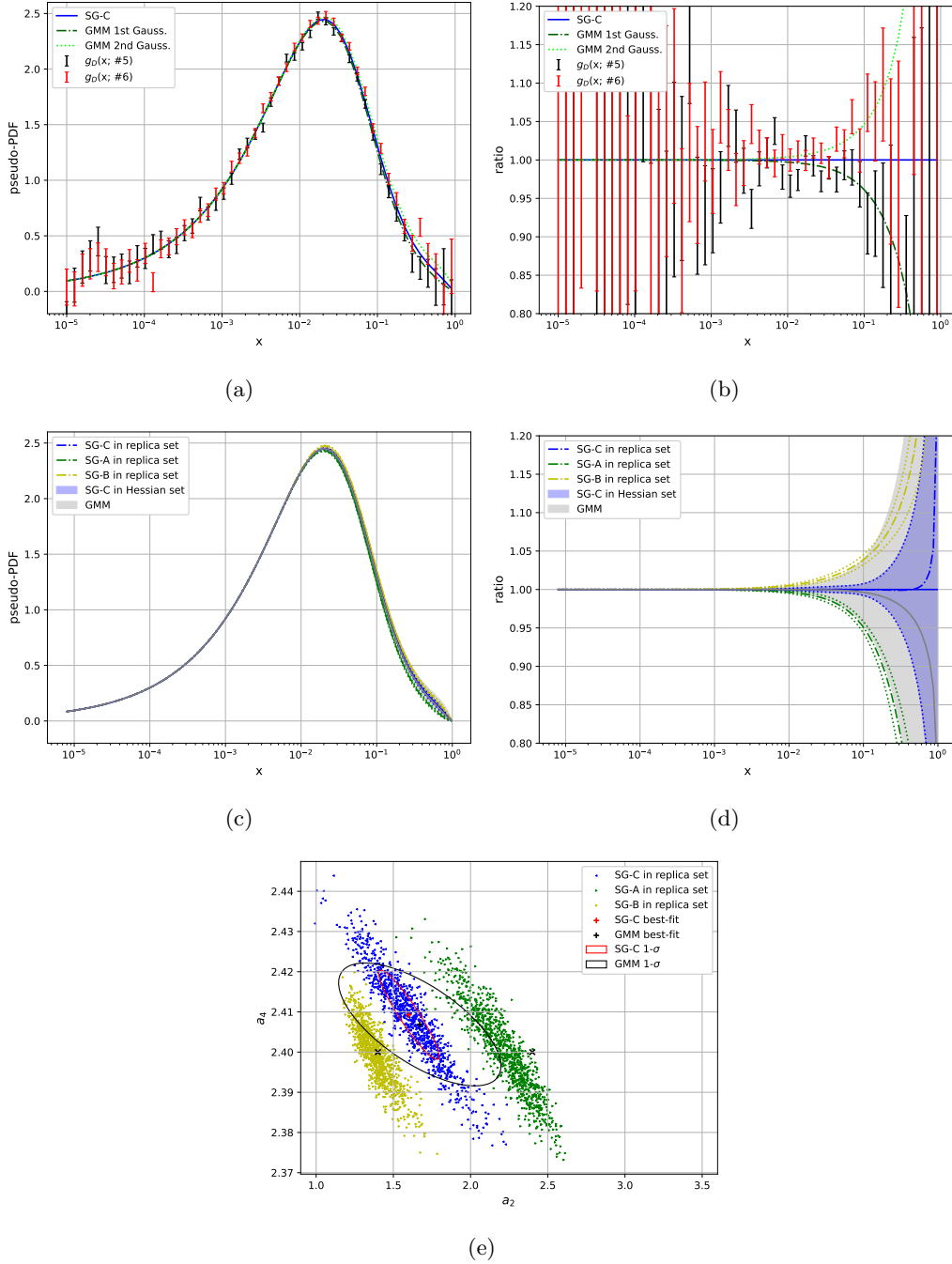


FIG. 6. Similar to Fig. 4, but for the Case-3.

two-tier (global+dynamic) tolerance (T) that accounts for theory, experimental, parametrization, and methodological uncertainties and results in error bands that are wider than the $\Delta\chi^2 = 1$ criterion. The CT Hessian uncertainty, at the 68% confidence level, nominally corresponds to $T^2 \equiv \Delta\chi_{total}^2 \approx 37$, where χ_{total}^2 is the sum of the global χ^2 and the so-called Tier-2 (dynamic) penalty [36, 37]. The MSHT PDF fits by default apply the “dynamic tolerance” procedure, as

detailed in [2, 38, 39]. This enlarges the uncertainties beyond the $\Delta\chi^2 = 1$ definition to account for data sets with tension, as well as potential mismatch of data and theory due to imprecision in the theory or parametrization and experimental measurements. The impact of different tolerance criteria on the determination of PDF induced uncertainties has been examined in Ref. [40]. In this study, we compare the results of applying the CT and MSHT tolerance criteria with $T^2 = 37$ to the ones with $\Delta\chi^2 = 1$.

The Hessian uncertainties based on the single Gaussian LS method with a tolerance criteria of $T^2 = 37$ for all three cases are compared to the GMM method in Figs. 7 to 9.

- Case-1: Both Hessian sets with CT and MSHT tolerance criteria estimate a smaller pseudo-PDF uncertainty for $10^{-3} < x < 0.1$, compared to the GMM. Recall for Case-1, the GMM produced a more faithful representation of uncertainties and overlapped with SG-A and SG-B. We see that the alternate tolerance criteria is not able to account for the larger uncertainties in this x range. Further, the uncertainties given by the modified tolerance criteria are much larger than required when $x > 0.1$. The same can also be observed in the fit parameter space. Here, the SG-C correlation ellipses with tolerance cover larger regions than the default Hessian set, but still cannot predict a correlation that spans regions of parameter space that cover portions of SG-A and SG-B.
- Case-2: As shown in Fig. 8, the larger tolerance leads to an overestimation of pseudo-PDF uncertainty, particularly for $x > 0.1$. In fact, the correlation ellipse for the larger tolerance, seen in the fit parameter space, has regions that are not populated by any of the replica sets.
- Case-3: As shown in Fig. 9(b), the GMM uncertainty (gray shaded regions of the pseudo-PDF ratios) shows better agreement with the uncertainty bands of the higher tolerance criteria. However, when comparing results in the fit parameter space, shown in Figs. 9(a), there appears to be significant mismatch between the higher tolerance ellipse and the GMM ellipse.

The tolerance criteria, currently in use by PDF collaborations, was introduced to capture larger uncertainties when there is tension in the fits. However, these methods are still based on the assumption that the likelihood behaves like a single Gaussian and is uni-modal. The tolerance criteria are not able to faithfully capture the effect of tension in the data. In some regions, the higher tolerance underestimates the uncertainty, and in others it overestimates the uncertainty.

The GMM, on the other hand, is able to provide a more faithful representation of the combined likelihoods of two data sets with tension.

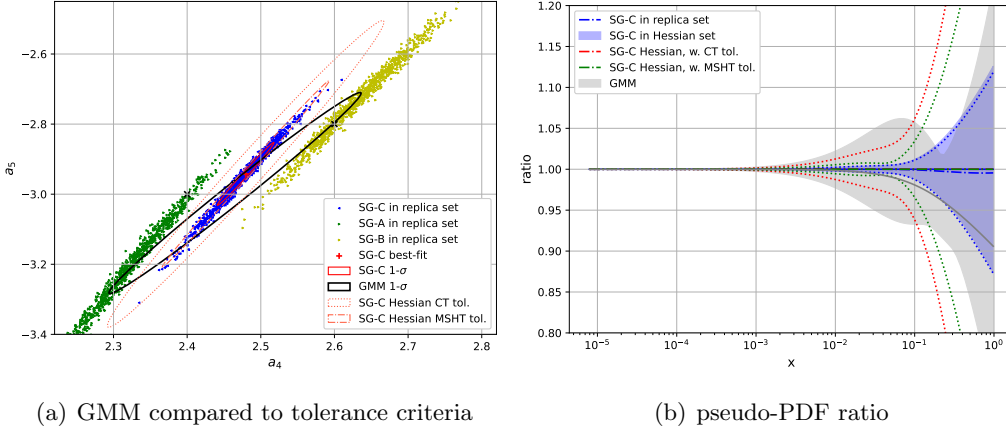


FIG. 7. The pseudo-PDF uncertainty estimated by the GMM method in Case-1 is compared to pseudo-PDF uncertainties predicted by the LS method along with the CT and MSHT tolerance criteria.

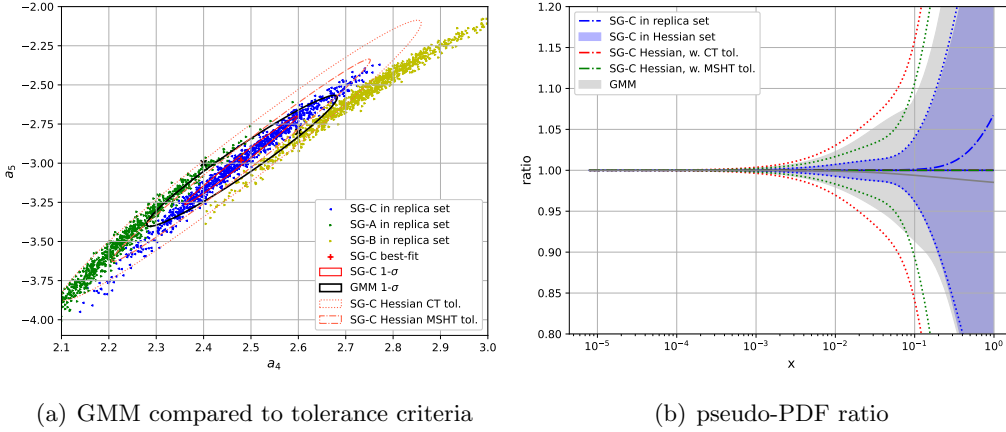


FIG. 8. Similar to Fig. 7, but for the Case-2.

V. CONSISTENCY CHECKS FOR THE GMM

In Sec. IV, we demonstrated how the GMM with two base Gaussian distributions is able to successfully describe the combined likelihood of two pseudo-data sets with tension. In this section, we show how the GMM reduces to the usual single Gaussian LS method when data are consistent. Further, as with any present day machine learning technique, when implementing the GMM, one

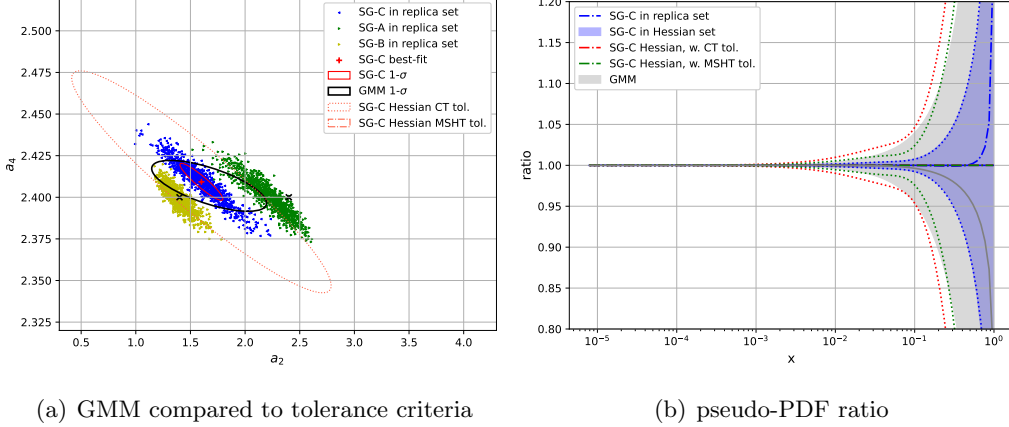


FIG. 9. Similar to Fig. 7, but for the Case-3.

must deal with over-fitting. In this section, we also remark on the consequences of over-fitting with the GMM.

V.1. Consistent results from consistent data

In Sec. III, we have shown how the GMM likelihood function reduces to the LS method when the number of Gaussians used in the GMM is $K = 1$. Another possibility for reducing to the usual χ^2 fit is when all base Gaussians end up with the same mean and covariance, i.e.

$$\mathbb{E}[\theta] \sim \hat{\theta}_i \sim \hat{\theta}_k, \quad \text{cov}_{\text{GMM},i} \sim \text{cov}_{\text{GMM},k}, \quad \text{and} \quad \mathcal{N}(y_j, \Delta y_j | \theta_i) \sim \mathcal{N}(y_j, \Delta y_j | \theta_k).$$

Consequently, the second term in Eq. (3.18), which accounts for the difference of means, vanishes. In this scenario, the covariance of the GMM reduces to

$$\begin{aligned} \text{cov}_{\text{GMM}} &\simeq \sum_{i=1}^K \omega_i \left(\sum_{j=1}^{N_{\text{pt}}} \left[-\frac{1}{\pi_j} \frac{\partial^2 \mathcal{N}_{ij}}{\partial \theta_i^2} + \frac{\omega_i}{\pi_j^2} \left(\frac{\partial \mathcal{N}_{ij}}{\partial \theta_i} \right)^2 \right] \right)^{-1} + \sum_{i=1}^K \omega_i (\mathbb{E}[\theta] - \hat{\theta}_i)^2 \\ &\simeq \left(\sum_{j=1}^{N_{\text{pt}}} \frac{1}{\Delta y_j^2} \right)^{-1}, \end{aligned} \quad (5.1)$$

which is the covariance found by the LS method in Eq. (3.15). When fitting a consistent data set, consistency between the GMM method and LS method are expected as shown analytically in Eq. (5.1). In practice, due to overfitting, we will see that the GMM reduces to the LS method only if no local minima exist in the log-likelihood, i.e. there is only one minimum of the log-likelihood.

Here, we verify Eq. (5.1) by performing two more fits on pseudo-data sets, as shown in Fig. 10:

- Case-4: This case concerns a fit to the pseudo-data # 7, which has the same truth as pseudo-data # 1, but without any statistical fluctuations. In this case, only a single extremum of the log-likelihood of the GMM exists, i.e. $\theta_i = \theta_k$, and we shall see that numerically as well, the GMM will reduce to the LS method fit.
- Case-5: This case concerns a fit to the pseudo-data # 1. Here, due to overfitting, we will see that although $\theta_i \simeq \theta_k$, the GMM tends to find multiple possible values of θ_k . This in turn implies that the results from the GMM method are different from the LS method.

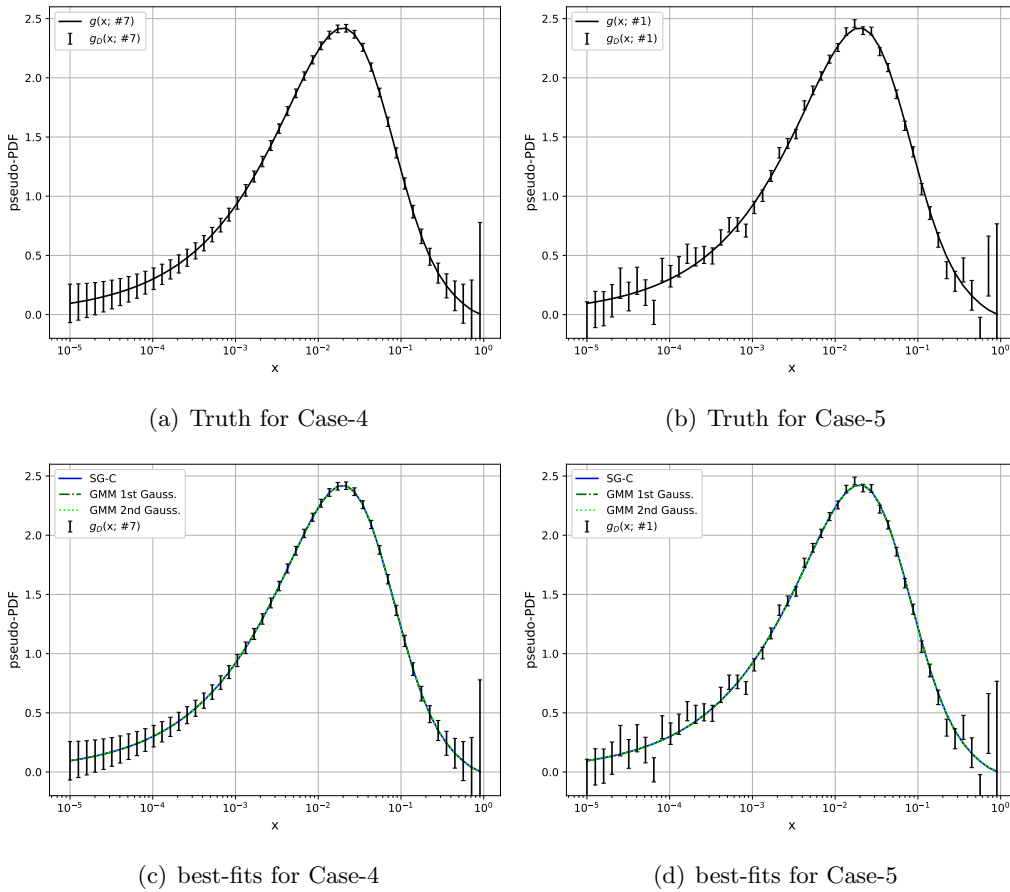


FIG. 10. Upper panels: the truths are compared to pseudo-data for Case-4 and Case-5. Lower panels: the best-fit pseudo-PDFs are compared to pseudo-data for both cases.

We begin by looking at results from the fit in Case-4. The uncertainties predicted by both methods are shown in Figs. 11(a), 11(c), 12(a), and 12(c). The figures indicate, as expected, that the central value of the fit for both the GMM and the LS methods are in good agreement. In Fig. 11(b) and Fig. 11(c), we see that the ellipses from the covariance matrix estimated using

both the GMM and the LS methods overlap and are identical. On the other hand, for Case-5, we notice in Fig. 11(b) and Fig. 11(d), that the covariance predicted by the GMM method cov_{GMM} is marginally larger than the covariance given by the LS method cov_{χ^2} . Fig. 11(d) shows that the covariance of individual base Gaussian distributions of the GMM $\text{cov}_{\text{GMM},i}$, which is larger than that obtained by the LS method cov_{χ^2} , and that the optimal values of parameters $\hat{\theta}_i$ for both base Gaussian distributions of the GMM differ by a small amount. The overestimation of uncertainty is a result of overfitting in GMM, where the GMM ends up learning statistical fluctuations rather than real tension between data sets.

The GMM method looks for tension and tries to categorize data into two or more different Gaussians. In general, for the GMM, overfitting gives rise to larger uncertainties and in that sense the GMM always provides a conservative estimate of the uncertainty.⁸ However, one would like to provide a precise PDF which is essential for the physics goals of the community. In order to determine if there is overfitting in the GMM, we describe certain information criteria in the next section that can be used to determine the optimal number of Gaussians, *i.e.*, the value of K . The result of Case-5 suggest that applying the GMM to a consistent data set will lead to larger uncertainties, which although conservative, should also be avoided.

V.2. Information Criteria for an Optimal number of base Gaussians

The results shown in Sec. V.1 indicate that the GMM method might over-estimate the uncertainty, especially if one includes more base Gaussian distributions than needed. Therefore, a procedure to determine the optimal value of K , for a mixture of K base Gaussian distributions of the GMM, is required. Here, we propose the use of the Akaike information criterion (AIC) [41] and Bayesian information criterion (BIC) [42] as indicators that will help determine optimal values for K , *i.e.*, the number of Gaussians. The values of AIC and BIC, defined in Eq. (5.2), increase as more parameters are introduced. They also take into account the change in goodness of fit and reduce as the fit improves. Both AIC and BIC are thus able to account for the trade-off between introducing additional parameters and an improvement to the fit. The minimum values for the AIC and BIC indicate to us the best choice of parameters, in this case, the best choice for the value

⁸ This is in contrast to overfitting by increasing the number of fit parameters in a LS fit, where overfitting may lead to a reduction in $\chi^2/N_{\text{pt}} < 1$. In this sense, the GMM method provides conservative estimates of the uncertainty.

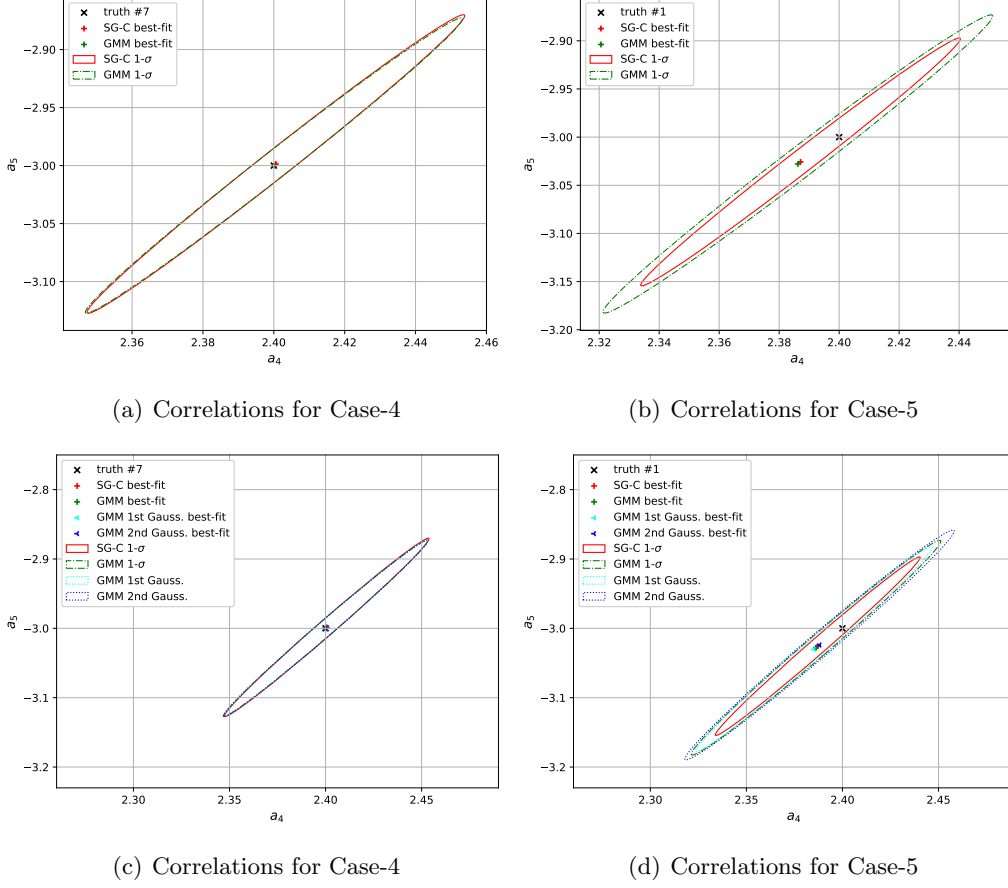


FIG. 11. Upper panels: the comparison of covariances obtained by the GMM method and the LS method, for the Case-4 and Case-5. Lower panels: similar to upper panels, but include the covariances of individual base Gaussian distributions of the GMM.

of K . The AIC and BIC are defined as

$$\begin{aligned} \text{AIC} &= N_p \ln N_{\text{pt}} - 2 \ln L|_{\theta=\hat{\theta}}, \\ \text{BIC} &= 2N_p - 2 \ln L|_{\theta=\hat{\theta}}. \end{aligned} \quad (5.2)$$

We count the number of independent parameters N_p for the GMM as following,

$$N_p = K \times N_{\text{param}} + (K - 1), \quad (5.3)$$

where N_{param} is the number of independent parameters for each base Gaussian distribution. The first term in Eq. (5.3) is the total number of fitting parameters over K copies of base distributions. The second term corresponds to the number of independent weights. In our pseudo-data study, there are always two free variables in the pseudo-PDF parametrization. Hence the total number of

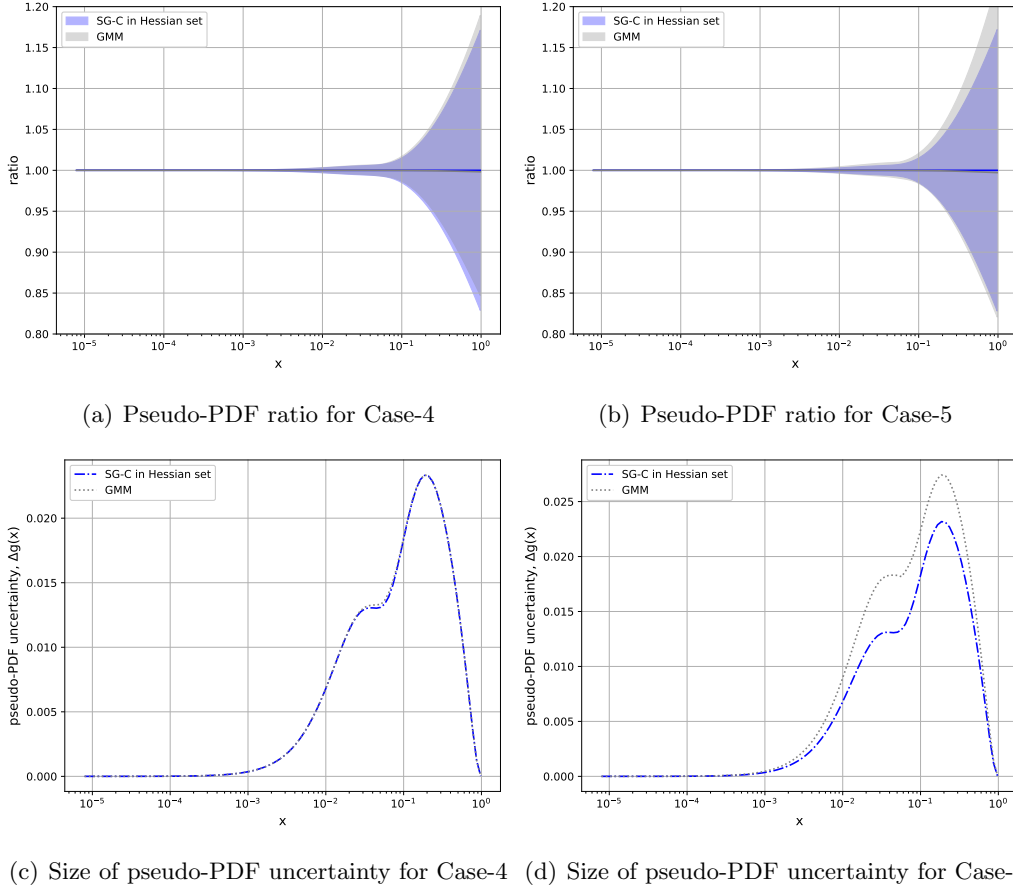


FIG. 12. Upper panels: the comparison of pseudo-PDF ratio obtained by both methods for Case-4 and Case-5, given the reference being the central value obtained by the LS method. Lower panels: the comparison of the sizes of pseudo-PDF uncertainty obtained by the GMM method and the LS method, for Case-4 and Case-5.

independent parameters for the GMM method in our current fits is

$$N_{\text{param}} = 2K + (K - 1). \quad (5.4)$$

We scan the AIC and BIC of the GMM up to $K = 4$ for all 5 cases considered in this work, as summarized in Table V. For Case-1 and Case-3, both AIC and BIC suggest two base Gaussian distributions would be optimal in order to faithfully extract information from their pseudo-data sets. This confirms the results shown in Sec. IV, particularly in Figs. 4(e) and 6(e), where two base Gaussian distributions can estimate a correlation that covers the two pseudo-data sets in tension. The AIC and BIC suggest for Case-2 a single Gaussian distribution is enough to fit this pseudo-data set. In Fig. IV.1, the LS method predicts a correlation, whose slope is close to the correlation estimated with two base Gaussian distributions. This is consistent with the fact that Case-2 has

minimal tension due to the large values of data errors. At this point we would like to point out that the GMM in conjunction with AIC and BIC, can be used to determine how much the errors in the data should be inflated in order to make them consistent so that we can use the LS method, as suggested in Ref. [16, 26–29].⁹ For Case-4 and Case-5, the AIC and BIC of course suggest that there is no need of using the GMM method, since by doing so one is over-fitting the data. We reiterate that the consequence of over-fitting is to increase our uncertainty and therefore leads to a conservative estimate of uncertainty, *i.e.*, using the optimum value of K provides the most precise PDFs, whereas larger values of K will lead to PDFs with larger uncertainty. We also notice in Table V that a higher number of base distributions K sometimes would lead to equal or slightly lower value of $-\ln L$ than the K suggested by AIC and BIC, indicating that one can equally or even better fit the data with more base distributions. However this is likely due to over-fitting the statistical fluctuations in the data. To conclude, although the GMM method is expected to reduce to the LS method for a consistent data set, one should avoid using it without detailed assessment of the level of tension. The combination of AIC and BIC indicators with the generalized statistical model of the GMM method could effectively reproduce the correct correlation in the presence of inconsistency in data. At the same time we can determine optimal values of K and provide a formalism to determine more precise PDFs.

VI. CONCLUSION

An accurate PDF uncertainty estimation is a theoretical necessity for precision measurements as well as new physics searches at the LHC and future colliders. The sources of PDF uncertainty include the theoretical uncertainty, the experimental systematic errors, and the sampling of PDF functional forms and fitting methodologies, etc. [35]. The existence of tension among different data sets can also reduce the precision of PDFs and necessitates the use of alternate statistical models that provide more accurate estimates of uncertainty. In this work, we described a formalism that generalizes the commonly used Least-Squares (LS) method and provides a way to combine likelihoods from different experiments in a statistically robust and meaningful way.

The proposed generalized likelihood modeled via the Gaussian mixture model (GMM) includes the possibility of the likelihood being either multi-modal or uni-modal. We demonstrated the shortcomings of the LS model when dealing with data sets that are in tension, using a toy model of

⁹ Specifically, one possible measure is to increase the errors in the data sets until the AIC and BIC indicate that $K = 1$ is the optimal value of K . This provides an alternate way to determine the scale factor used in Ref. [26].

		$K = 1$	$K = 2$	$K = 3$	$K = 4$
Case-1	AIC	-102.2	-203.6	-194.9	-187.9
	BIC	-106.1	-211.2	-206.4	-203.2
$N_{\text{pt}}=100$	$-\ln L$	-55.0	-109.6	-109.2	-109.6
Case-2	AIC	-21.2	-15.4	-7.9	-0.2
	BIC	-25.0	-23.0	-19.3	-15.5
$N_{\text{pt}}=100$	$-\ln L$	-14.5	-15.5	-15.7	-15.7
Case-3	AIC	-219.3	-220.2	-212.8	-205.0
	BIC	-223.2	-227.8	-224.3	-220.3
$N_{\text{pt}}=100$	$-\ln L$	-113.6	-117.9	-117.9	-118.1
Case-4	AIC	-117.8	-109.9	-102.1	-94.3
	BIC	-121.6	-117.6	-113.6	-109.6
$N_{\text{pt}}=50$	$-\ln L$	-62.8	-62.8	-62.8	-62.8
Case-5	AIC	-169.3	-161.5	-153.6	-145.8
	BIC	-173.1	-169.1	-165.1	-161.1
$N_{\text{pt}}=50$	$-\ln L$	-88.6	-88.6	-88.6	-88.6

TABLE V. The AIC, BIC and $-\ln L$ for Case-1 to Case-5 obtained by the GMM with various numbers of base distributions. The lowest values of AIC, BIC and $-\ln L$ for each cases are written in bold font.

PDFs. We found that, with a single Gaussian distribution assumed in the LS method, neither the Monte Carlo method nor the Hessian method can provide an accurate sampling of the probability distribution of the pseudo PDFs. Although the Monte Carlo method directly samples the probability distribution in the data space, the assumption that there is only one Gaussian distribution in the PDF space leads to a LS fit that would be stuck in a narrow valley of χ^2 . The same situation applies to the Hessian method. Inflating the Hessian uncertainty with certain tolerance criteria is a conservative prescription for the uncertainty estimation currently used by PDF fitting collaborations. We find that doing so is not a guarantee of a good approximation of the combined likelihood of two data sets that are in tension, particularly in the case where the tension is complicated. Specifically, the value of the tolerance chosen is not based on statistically robust arguments. Further, we showed how increasing the tolerance does not accurately capture tension and leads to inadequate uncertainty in some regions of the PDF but at the same time an overestimation of uncertainty in other regions of the PDF, c.f. Fig. 4(d). This can also be seen in the correlation ellipses of the fit parameter space. What is required here is not just an extension of the original χ^2

ellipse, but also a rotation of the axes of the correlation ellipse. The latter can neither be achieved with a modified tolerance criteria nor by using a Monte-Carlo sampling technique.

The novel GMM pseudo-PDF fit overcomes these shortcomings of the LS method by parametrizing the likelihood as a mixture of Gaussian distributions, by allowing for a multi-modal feature of the likelihood. We have described how this unsupervised machine learning technique can be leveraged to learn about tension in the fits as well as be used to determine precisely the uncertainties on the PDFs. Specifically, it is possible to use the GMM for performing the unsupervised machine learning task of clustering the data in order to identify and learn about the tension in the data sets. We have demonstrated how the GMM is simply generalization of the χ^2 log-likelihood and reduces to it when data is consistent. Finally, It is possible to over-fit in the GMM, where the model might end up learning statistical fluctuations rather than real tension between data sets. We have described the use of the Akaike information criterion (AIC) and Bayesian information criterion (BIC) to avoid over-fitting and can be used to determine optimal value of the number of base distributions for the GMM method.

ACKNOWLEDGMENT

MY thanks Yandong Liu and Pavel Nadolsky for the discussions. MY has left PKU at the time of this paper being posted. This work was supported in part by the National Science Foundation of China under grants No. 12075251, and the Natural Science Foundation of Hunan province of China under Grant No. 2023JJ30496. It is also supported in part by the U.S. National Science Foundation under Grant No. PHY-2310291 and PHY-2310497.

-
- [1] T.-J. Hou *et al.*, “New CTEQ global analysis of quantum chromodynamics with high-precision data from the LHC,” [Phys. Rev. D **103** no. 1, \(2021\) 014013](#), [arXiv:1912.10053 \[hep-ph\]](#).
 - [2] S. Bailey, T. Cridge, L. A. Harland-Lang, A. D. Martin, and R. S. Thorne, “Parton distributions from LHC, HERA, Tevatron and fixed target data: MSHT20 PDFs,” [Eur. Phys. J. C **81** no. 4, \(2021\) 341](#), [arXiv:2012.04684 \[hep-ph\]](#).
 - [3] **NNPDF** Collaboration, R. D. Ball *et al.*, “The path to proton structure at 1% accuracy,” [Eur. Phys. J. C **82** no. 5, \(2022\) 428](#), [arXiv:2109.02653 \[hep-ph\]](#).
 - [4] S. Alekhin, J. Blümlein, S. Moch, and R. Placakyte, “Parton distribution functions, α_s , and heavy-quark masses for LHC Run II,” [Phys. Rev. D **96** no. 1, \(2017\) 014011](#), [arXiv:1701.05838](#)

- [hep-ph].
- [5] **ATLAS** Collaboration, G. Aad *et al.*, “Determination of the parton distribution functions of the proton using diverse ATLAS data from pp collisions at $\sqrt{s} = 7, 8$ and 13 TeV,” *Eur. Phys. J. C* **82** no. 5, (2022) 438, [arXiv:2112.11266](#) [hep-ex].
- [6] **NNPDF** Collaboration, R. D. Ball *et al.*, “An open-source machine learning framework for global analyses of parton distributions,” *Eur. Phys. J. C* **81** no. 10, (2021) 958, [arXiv:2109.02671](#) [hep-ph].
- [7] S. Alekhin *et al.*, “HERAFitter,” *Eur. Phys. J. C* **75** no. 7, (2015) 304, [arXiv:1410.4412](#) [hep-ph].
- [8] S. Amoroso *et al.*, “Snowmass 2021 whitepaper: Proton structure at the precision frontier,” *Acta Phys. Polon. B* **53** no. 12, (2022) A1, [arXiv:2203.13923](#) [hep-ph].
- [9] **CDF** Collaboration, T. Aaltonen *et al.*, “High-precision measurement of the W boson mass with the CDF II detector,” *Science* **376** no. 6589, (2022) 170–176.
- [10] M. Cepeda *et al.*, “Report from Working Group 2: Higgs Physics at the HL-LHC and HE-LHC,” *CERN Yellow Rep. Monogr.* **7** (2019) 221–584, [arXiv:1902.00134](#) [hep-ph].
- [11] **LHC Higgs Cross Section Working Group** Collaboration, D. de Florian *et al.*, “Handbook of LHC Higgs Cross Sections: 4. Deciphering the Nature of the Higgs Sector,” [arXiv:1610.07922](#) [hep-ph].
- [12] **ATLAS** Collaboration, M. Aaboud *et al.*, “Precision measurement and interpretation of inclusive W^+ , W^- and Z/γ^* production cross sections with the ATLAS detector,” *Eur. Phys. J. C* **77** no. 6, (2017) 367, [arXiv:1612.03016](#) [hep-ex].
- [13] T.-J. Hou, H.-W. Lin, M. Yan, and C. P. Yuan, “Impact of lattice $s(x) - \bar{s}(x)$ data in the CTEQ-TEA global analysis,” [arXiv:2204.07944](#) [hep-ph].
- [14] M. Guzzi *et al.*, “NNLO constraints on proton PDFs from the SeaQuest and STAR experiments and other developments in the CTEQ-TEA global analysis,” *SciPost Phys. Proc.* **8** (2022) 005, [arXiv:2108.06596](#) [hep-ph].
- [15] T.-J. Hou, M. Yan, J. Liang, K.-F. Liu, and C. P. Yuan, “Connected and disconnected sea partons from the CT18 parametrization of PDFs,” *Phys. Rev. D* **106** no. 9, (2022) 096008, [arXiv:2206.02431](#) [hep-ph].
- [16] K. Kovarič, P. M. Nadolsky, and D. E. Soper, “Hadronic structure in high-energy collisions,” *Rev. Mod. Phys.* **92** no. 4, (2020) 045003, [arXiv:1905.06957](#) [hep-ph].
- [17] **NNPDF** Collaboration, R. D. Ball, A. Candido, J. Cruz-Martinez, S. Forte, T. Giani, F. Hekhorn, K. Kudashkin, G. Magni, and J. Rojo, “Evidence for intrinsic charm quarks in the proton,” *Nature* **608** no. 7923, (2022) 483–487, [arXiv:2208.08372](#) [hep-ph].
- [18] R. Stegeman, “The negligible impact of experimental inconsistencies in the NNPDF4.0 global dataset,” *PoS ICHEP2022* (2022) 787, [arXiv:2212.07703](#) [hep-ph].

- [19] N. Lambri, “Optimized regression models for parton distribution functions determination using deep learning models,” 2020.
http://nnpdf.mi.infn.it/wp-content/uploads/2021/01/thesis_lambri.pdf.
- [20] L. Talon, “Optimization of parton density uncertainties,” 2019.
http://nnpdf.mi.infn.it/wp-content/uploads/2019/06/Talon_MS_thesis.pdf.
- [21] **PDF4LHC21 combination group** Collaboration, T. Cridge, “PDF4LHC21: Update on the benchmarking of the CT, MSHT and NNPDF global PDF fits,” *SciPost Phys. Proc.* **8** (2022) 101, [arXiv:2108.09099](https://arxiv.org/abs/2108.09099) [hep-ph].
- [22] H. Paukkunen and P. Zurita, “PDF reweighting in the Hessian matrix approach,” *JHEP* **12** (2014) 100, [arXiv:1402.6623](https://arxiv.org/abs/1402.6623) [hep-ph].
- [23] G. Cybenko, “Approximation by superpositions of a sigmoidal function,” *Mathematics of control, signals, and systems* **2** no. 4, (1989) 303–314.
- [24] M. H. Stone, “Applications of the theory of boolean rings to general topology,” *Transactions of the American Mathematical Society* **41** no. 3, (1937) 375–481.
- [25] M. H. Stone, “The generalized weierstrass approximation theorem,” 1948.
- [26] **Particle Data Group** Collaboration, R. L. Workman *et al.*, “Review of Particle Physics,” *PTEP* **2022** (2022) 083C01.
- [27] J. Erler and R. Ferro-Hernández, “Alternative to the application of PDG scale factors,” *Eur. Phys. J. C* **80** no. 6, (2020) 541, [arXiv:2004.01219](https://arxiv.org/abs/2004.01219) [physics.data-an].
- [28] G. Cowan, “Statistical Models with Uncertain Error Parameters,” *Eur. Phys. J. C* **79** no. 2, (2019) 133, [arXiv:1809.05778](https://arxiv.org/abs/1809.05778) [physics.data-an].
- [29] G. D’Agostini, “Sceptical combination of experimental results: General considerations and application to epsilon-prime / epsilon,” [arXiv:hep-ex/9910036](https://arxiv.org/abs/hep-ex/9910036).
- [30] K. Pearson, “Contributions to the mathematical theory of evolution,” *Philosophical Transactions of the Royal Society of London. A* **185** (1894) 71–110.
- [31] K. P. Murphy, *Machine learning: a probabilistic perspective*. MIT Press, Cambridge, MA, 2012.
- [32] M. Abadi, A. Agarwal, P. Barham, E. Brevdo, Z. Chen, C. Citro, G. S. Corrado, A. Davis, J. Dean, M. Devin, S. Ghemawat, I. Goodfellow, A. Harp, G. Irving, M. Isard, Y. Jia, R. Jozefowicz, L. Kaiser, M. Kudlur, J. Levenberg, D. Mane, R. Monga, S. Moore, D. Murray, C. Olah, M. Schuster, J. Shlens, B. Steiner, I. Sutskever, K. Talwar, P. Tucker, V. Vanhoucke, V. Vasudevan, F. Viegas, O. Vinyals, P. Warden, M. Wattenberg, M. Wicke, Y. Yu, and X. Zheng, “TensorFlow: Large-Scale Machine Learning on Heterogeneous Distributed Systems,” [arXiv:1603.04467](https://arxiv.org/abs/1603.04467).
- [33] K. Basford, D. Greenway, G. McLachlan, and D. Peel, “Standard errors of fitted component means of normal mixtures,” *Computational Statistics* **12** (01, 1997) 1.
- [34] H. M. Bücker and G. F. Corliss, “A bibliography on automatic differentiation,” in *Automatic Differentiation: Applications, Theory, and Implementations*, H. M. Bücker, G. F. Corliss, P. D.

- Hovland, U. Naumann, and B. Norris, eds., vol. 50 of Lecture Notes in Computational Science and Engineering, pp. 321–322. Springer, New York, NY, 2005.
- [35] A. Courtoy, J. Huston, P. Nadolsky, K. Xie, M. Yan, and C. P. Yuan, “Parton distributions need representative sampling,” [arXiv:2205.10444 \[hep-ph\]](#).
- [36] H.-L. Lai, M. Guzzi, J. Huston, Z. Li, P. M. Nadolsky, J. Pumplin, and C. P. Yuan, “New parton distributions for collider physics,” [Phys. Rev. D](#) **82** (2010) 074024, [arXiv:1007.2241 \[hep-ph\]](#).
- [37] J. Gao, M. Guzzi, J. Huston, H.-L. Lai, Z. Li, P. Nadolsky, J. Pumplin, D. Stump, and C. P. Yuan, “CT10 next-to-next-to-leading order global analysis of QCD,” [Phys. Rev. D](#) **89** no. 3, (2014) 033009, [arXiv:1302.6246 \[hep-ph\]](#).
- [38] A. D. Martin, W. J. Stirling, R. S. Thorne, and G. Watt, “Parton distributions for the LHC,” [Eur. Phys. J. C](#) **63** (2009) 189–285, [arXiv:0901.0002 \[hep-ph\]](#).
- [39] L. A. Harland-Lang, A. D. Martin, P. Motylinski, and R. S. Thorne, “Parton distributions in the LHC era: MMHT 2014 PDFs,” [Eur. Phys. J. C](#) **75** no. 5, (2015) 204, [arXiv:1412.3989 \[hep-ph\]](#).
- [40] X. Jing *et al.*, “Quantifying the interplay of experimental constraints in analyses of parton distributions,” [Phys. Rev. D](#) **108** no. 3, (2023) 034029, [arXiv:2306.03918 \[hep-ph\]](#).
- [41] H. Akaike, “A new look at the statistical model identification,” [IEEE Transactions on Automatic Control](#) **19** no. 6, (1974) 716–723.
- [42] G. Schwarz, “Estimating the Dimension of a Model,” [The Annals of Statistics](#) **6** no. 2, (1978) 461 – 464. <https://doi.org/10.1214/aos/1176344136>.